IEEE Access
Multidisciplinary ⋮ Rapid Review ⋮ Open Access Journal

Received October 5, 2021, accepted October 18, 2021, date of publication October 26, 2021, date of current version November 2, 2021.

Digital Object Identifier 10.1109/ACCESS.2021.3122920

Filtered PID Control Loop for Third Order Plants With Delay: Dominant Pole Placement Approach

JAROMÍR FIŠER[1,2] AND PAVEL ZÍTEK[1]

[1]Department of Instrumentation and Control Engineering, Faculty of Mechanical Engineering, Czech Technical University in Prague, 166 07 Prague, Czech Republic

[2]Center of Advanced Aerospace Technology, Faculty of Mechanical Engineering, Czech Technical University in Prague, 166 07 Prague, Czech Republic

Corresponding author: Jaromír Fišer (jaromir.fiser@fs.cvut.cz)

Authors acknowledge support from the ESIF, EU Operational Programme Research, Development and Education, and from the Center of Advanced Aerospace Technology (CZ.02.1.01/0.0/0.0/16_019/0000826), Faculty of Mechanical Engineering, Czech Technical University in Prague.

ABSTRACT The paper deals with tuning the filtered PID controller applied to third order plants with delay. This model option is chosen as a representative case where the loop characteristic quasi-polynomial is of higher order than three. Applying the similarity theory for introducing dimensionless parameterization a comparative model of third order plant dynamics is obtained. Four dominant poles – from the infinite spectrum of the control loop – are assigned by means of tuning three controller gains and a filter time constant where a specific argument increment criterion proves their dominance. The pole prescription coordinates are parameterized via damping, root and natural frequency ratios optimized in the space of the introduced similarity numbers according to the IAE criterion with respect to robustness and filtering constraints. Particularly the natural frequency ratio is a new parameter introduced to tune robustly the PID together with its filter. For the constrained IAE optimization the response of disturbance rejection is used as a representative of control loop behavior. In the space of similarity numbers of the plant it is shown that a limited range of plants is suited to be controlled on the PID control principle and the boundaries of this range are outlined. Survey maps of optimum controller parameters are presented and a comparative study on benchmark application example is added.

INDEX TERMS Control design, delay systems, filtering, robustness, similarity theory.

I. INTRODUCTION

In industry the most frequent output driven control is provided by a PID-type structure controller, even for systems with significant time delay [1]. There are many PI(D) tuning rules for the first- or second-order plants with a delay which is regularly approximated by the Padé or Taylor series [2]–[7]. Predominantly these tunings are based on ultimate cycle identification, various performance index minimizations, gain, phase and jitter margin specifications, magnitude optimum method, pole placement technique or IMC-like tuning (so-called Lambda tuning), which are particularly well suited for non-dominant delay processes, except for the IMC-like tuning, [8], and the dominant pole placement, [9]. The former tuning is suitable for dominant delay processes assuming safe pole-zero cancellation in the open loop [10], in [11] this cancellation is modified to systems with large time delay and in [12] the IMC-like PID with a second-order lead-lag filter compensates for the dominant plant poles and zeros. In [13] the Lambda tuning method is modified for integrating systems by the polynomial approach. The latter tuning is also applicable to the dominant delay processes but assuming no pole-zero cancellation within the control loop. In [14]–[16] the pole-zero matching method is applied to inexact dominant pole placement, which is free of any delay term approximation, and in [17] a universal map of PID tuning for the second-order processes with dominant delay is presented.

Generally, in tuning the PI(D) controllers a trade-off between the robustness and performance is searched, and moreover a trade-off between the reference tracking and disturbance rejection performance/robustness is subject to a controller optimization [18]–[20]. On one hand the robust PID tuning results in conservative setting at the expense of

The associate editor coordinating the review of this manuscript and approving it for publication was Zhiguang Feng.

minimization of performance indices like Integral Absolute Error (IAE), Integral Square Error (ISE) etc., [10]. On the other hand the PID controller optimized to the disturbance rejection can be hardly an optimum controller for the reference tracking. The trade-off tuning is tackled by the model matching approach to filtered PID design, [21], and in [20] the disturbance rejection performance with respect to the reference input level is guaranteed by keeping the so-called reference to disturbance ratio index as high as possible. Next, in [22] the proportional gain maximization method is introduced based on the optimizing the damping ratio of the controller zeros which resulted circa three quarters. With this result the control performance is improved without deteriorating the robustness to model uncertainties. To make the disturbance rejection and reference tracking mutually comparable the notion of extreme frequency equivalence is utilized [19], [23]. The reason of unfavorable disturbance rejection and reference tracking consists in a pole-zero cancellation within the control loop. Hence the tuning methods, particularly the Lambda tuning, [10], based on the pole-zero cancellation or methods, like gain and phase margins, [5], assuming the pole-zero cancellation are potentially inappropriate for the (load) disturbance rejection task. Nevertheless, the lambda tuning for given (load) disturbance is obtainable with effective disturbance rejection [12], [24]. To prevent from dominant pole(s) cancellation in case of the reference tracking a two-degree-of-freedom control loop is proposed, [25], or an input prefilter is designed [26]. Measurement noise filter of the second order is designed for mitigating abrupt control actions [27] and in [28] the higher-order noise filters are tuned. In [29] the measurement noise filter tuning is provided for common PID tuning rules in case of reduced order plant model. Based on the filter from [27] the filtered PID control loop is tuned up for the second-order plant with delay by the dominant four-pole placement in [30]. In practice a filter time constant setting obeys a rule of thumb, fixing the derivative time constant ratio to the filter time constant, [8]. As opposed to the rule of thumb, constraining above mentioned ratio due to the loop cut-off frequency and the demand on high-frequency control sensitivity the PID tuning obtains benefits like disturbance rejection capability, phase margin increase and controller frequency band extension [31]. On the other hand a priori tuned filter time constant can contribute to excessive high-frequency control sensitivity to be avoided in practice.

In practice it is a difficult task to identify higher-order plant dynamics hence a model order reduction is imposed on a controller design [24], [32]. In case of higher-order systems with time delay the dominant pole placement in conjunction with the D-partition method is presented in [1]. Comparative studies in [33], [34] compares simple PID tuning rules and methods, where a derivative part filter is in action, provided for higher-order non-oscillating plants or plants with significant delay. As regards the third-order plants with delay the tuning rules are developed in analogous way, [2], that are not frequently applied in literature. One of them is the IMC-like tuning, [35], considered for the third-order plants. In studies [36], [37] all the stabilizing PID controller settings obtained are eligible only to a fixed third-order plant with delay and these settings do not guarantee satisfactory control performance in general. In [38] all the stabilizing PID controllers obtained are extended to more general class of delay systems and a survey on all the stabilizing PID controller designs are presented in [39]. Typically, the plants of the third order are thermal [40], water or wind power plants, [41] or [42] respectively. From application point of view the most difficult is to reject loads or disturbances of plants providing energy conversion, for instance [43], [44]. In [45] a universal adaptive controller design applicable to the first- through third-order plants is presented. Frequently the third-order plant model describes the second-order plant dynamics but with additional, not negligible actuator dynamics, [46], [47]. For higher-order systems the test benchmark models can be found in [48]–[50]. The third-order plants with a delay are apparently present in the industry and therefore any other order reduction means inappropriate approximation.

In the paper the universal PID and filter settings are proposed with the aim to get optimum controller gains and filter time constant with respect to not only the IAE criterion but also to robustness and filtering effect constraints. Besides the damping and root ratio prescription, these settings are based on finding the ratio between two natural frequencies prescribed where the greater one is the ultimate frequency of the plant. The novelty of the dominant pole placement approach consisting in the frequency ratio prescription brings robust PID and filter settings for the sets of dynamically similar third-order plants with delay. Without finding an optimum frequency ratio the four-pole dominance would be barely guaranteed. Finally, the optimum controller and filter parameters are mapped to show varying delay effect.

II. THIRD ORDER PLANT MODEL PARAMETERIZATION

As presented in the Introduction the third-order plants with delay are commonly identified in the industry. Such plants are modelled by the following third-order model with delay

$$c_3\frac{d^3y(t)}{dt^3}+c_2\frac{d^2y(t)}{dt^2}+c_1\frac{dy(t)}{dt}+y(t)=Ku(t-\upsilon) \qquad (1)$$

where $y(t)$ and $u(t)$, output and input variables respectively, are expressed as dimensionless percentage of the sensor and actuator instrument ranges. The coefficients c_1, c_2, c_3 and the delay value υ are supposed positive dimensional constants and K is a nonzero dimensionless steady state gain. From the plant transfer function

$$G(s)=\frac{K}{\tilde{M}(s)}\exp(-s\upsilon), \quad \tilde{M}(s)=c_3s^3+c_2s^2+c_1s+1 \quad (2)$$

it follows that the *only three poles* of the plant are the roots of the characteristic equation $\tilde{M}(s)=0$. Dividing $\tilde{M}(s)$ by c_3 the characteristic polynomial can be identified with the root

factor product form as follows

$$M(s) = (s-q_1)(s-q_2)(s-q_3) = \tilde{M}(s)\Big/c_3 = s^3-(q_1+q_2+q_3)\,s^2+(q_1q_2+q_2q_3+q_1q_3)\,s-q_1q_2q_3 = 0 \quad (3)$$

The following *two stable* options of the $M(s)$ roots are further considered

$$q_1 = -b,\ q_2 = -\chi_1 b,\ q_3 = -\chi_2 b, b > 0,\ \chi_{1,2} > 0, \quad (4)$$

$$q_{1,2} = (-\xi \pm j\eta)\,\omega_n, q_3 = -\chi\xi\omega_n,\ \eta = \sqrt{1-\xi^2},\ \omega_n > 0,\ 0 < \xi \le 1, \chi > 0 \quad (5)$$

where ω_n is the natural frequency and ξ is the damping factor of complex conjugates $q_{1,2}$. Positive constant b is the absolute value of real pole q_1 and $q_{2,3} = \chi_{1,2}q_1$ are other two distinct real poles. The special case of double real pole and one single real pole belongs to option (5) when $\xi = 1$, and the case of triple real pole belongs to option (4) with $\chi_{1,2} = 1$.

For further modification of the plant model the parameterization principle introduced by Vyshnegradskii, [51], is used. Analogously to [17] the following dimensionless substitution for Laplace transform variable is introduced

$$\bar{s} = s\sqrt[3]{c_3} \quad (6)$$

to achieve the characteristic polynomial (3) in the form

$$M(\bar{s}) == \bar{s}^3+\frac{c_2}{\sqrt[3]{c_3^2}}\bar{s}^2+\frac{c_1}{\sqrt[3]{c_3}}\bar{s}+1 = \bar{s}^3+\frac{1}{\lambda_2}\bar{s}^2+\frac{1}{\lambda_1}\bar{s}+1 \quad (7)$$

Instead of three coefficients c_1, c_2, c_3 only two dimensionless parameters

$$\frac{1}{\lambda_1} = \frac{c_1}{\sqrt[3]{c_3}}, \quad \frac{1}{\lambda_2} = \frac{c_2}{\sqrt[3]{c_3^2}} \quad (8)$$

determine the character of the plant dynamics. Due to their independence of the time scale of the considered case λ_1, λ_2 can serve as *similarity numbers* of the plant dynamics. For the types (4) and (5) of plants, relations (8) lead to the particular relationships distinguished by the *discriminant* of cubic equation $M(\bar{s}) = 0$

$$D = 4\left(\frac{1}{\lambda_1^3}+\frac{1}{\lambda_2^3}\right)-\frac{1}{\lambda_1^2\lambda_2^2}-\frac{18}{\lambda_1\lambda_2}+27 \quad (9)$$

First, for *aperiodic plants*, i.e. for option (4) when $D \le 0$, the coefficients in (3) are given by the poles $q_{1,2,3}$ coordinates in the following way

$$\frac{1}{c_3} = \chi_1\chi_2 b^3,\ \frac{c_2}{c_3} = (1+\chi_1+\chi_2)\,b,\ \frac{c_1}{c_3} = (\chi_1+\chi_2+\chi_1\chi_2)\,b^2 \quad (10)$$

Substitution (6) leads in this case to relation $s = \bar{s}b\sqrt[3]{\chi_1\chi_2}$ which gives the following form of (8)

$$\frac{1}{\lambda_1} = \frac{\chi_1+\chi_2+\chi_1\chi_2}{\sqrt[3]{\chi_1^2\chi_2^2}}, \quad \frac{1}{\lambda_2} = \frac{1+\chi_1+\chi_2}{\sqrt[3]{\chi_1\chi_2}} \quad (11)$$

and the pole option (4) is expressed as $q_{1,2,3} = \bar{q}_{1,2,3}b\sqrt[3]{\chi_1\chi_2}$. The triple real pole, $\chi_{1,2} = 1$, is encountered when $D = 0$ and this case corresponds to the similarity number option $\lambda_{1,2} = 1/3$. For the oscillatory plants, i.e. for option (5) when $D > 0$, the coefficients of $M(s)$ are given by the poles $q_{1,2,3}$ coordinates as follows

$$\frac{1}{c_3} = \chi\xi\omega_n^3, \quad \frac{c_2}{c_3} = (\chi+2)\,\xi\omega_n, \quad \frac{c_1}{c_3} = \left(2\chi\xi^2+1\right)\omega_n^2 \quad (12)$$

Substitution (6) here results in $\bar{s}\omega_n\sqrt[3]{\chi\xi} = s$ and leads to the coefficients of $M(\bar{s})$ determined by the ratios χ, ξ only

$$\frac{1}{\lambda_1} = \frac{2\chi\xi^2+1}{\sqrt[3]{\chi^2\xi^2}}, \quad \frac{1}{\lambda_2} = \frac{\xi(\chi+2)}{\sqrt[3]{\chi\xi}} \quad (13)$$

The pole option (5) is now expressed by $q_{1,2,3} = \bar{q}_{1,2,3}\omega_n\sqrt[3]{\chi\xi}$. In both types of plants parameters λ_1, λ_2 are independent of coordinates b and ω_n, respectively. In the case of oscillatory plants similarity numbers λ_1, λ_2 express the degree of *oscillability*, so they are further referred to as *oscillability numbers*. Higher values of λ_1, λ_2 mean less damped natural oscillation.

Plant (1) is considered as stable and therefore coefficients c_1, c_2, c_3 are not only positive but are to satisfy the stability condition, $c_1c_2-c_3 > 0$, coming from Hurwitz criterion applied to plant model (2). Expressing the product of two relations in (8) the similarity numbers satisfy for stable plants the following condition

$$c_1c_2 = \frac{c_3}{\lambda_1\lambda_2} > c_3 \rightarrow \lambda_1\lambda_2 < 1 \quad (14)$$

Parameters λ_1, λ_2 describe only the dynamics given by the characteristic polynomial $M(s)$ of plant (1). Nevertheless, it is necessary to be aware of the essential influence of the *delay* on the plant dynamic properties in closing the feedback loop. From substitution (6) the substitution for time variable, $\bar{t} = t/\sqrt[3]{c_3}$, results. Thus, the delay length is expressed by the ratio

$$\vartheta = \frac{\upsilon}{\sqrt[3]{c_3}} \quad (15)$$

and this delay parameter is further referred to as *laggardness* number of the plant. Using the introduced similarity numbers the plant model (1) is transformed to the form

$$\frac{d^3y(\bar{t})}{d\bar{t}^3}+\frac{1}{\lambda_2}\frac{d^2y(\bar{t})}{d\bar{t}^2}+\frac{1}{\lambda_1}\frac{dy(\bar{t})}{d\bar{t}}+y(\bar{t}) = Ku(\bar{t}-\vartheta) \quad (16)$$

The advantage of this form of model consists in the property that all dynamically similar plants fall into one common point of the λ_1, λ_2, ϑ and K parameter space from where steady-state gain K can be still excluded as shown below.

III. DIMENSIONLESS CONTROL LOOP DESCRIPTION

The third-order plant with delay given by model (1) or (16) is controlled by the following ideal PID controller

$$\frac{du(t)}{dt} = r_P\frac{de_f(t)}{dt}+r_D\frac{d^2e_f(t)}{dt^2}+r_Ie_f(t) \quad (17)$$

where e_f is the filtered control error. The filtering is provided by the solution of the following first-order differential equation

$$T_f \frac{de_f(t)}{dt} + e_f(t) = e(t) \tag{18}$$

where $e = w_f - y$, w_f is the prefiltered reference variable. Beside the control error filtering the reference variable is prefiltered to prevent from the excitation of high-frequency unmodeled dynamics. Then the following second-order differential equation is considered

$$r_D \frac{d^2 w_f(t)}{dt^2} + r_P \frac{dw_f(t)}{dt} + r_I w_f(t) = r_I w(t) \tag{19}$$

where w is the reference variable in percentage again and $r_P > 0$, $r_D > 0$, $r_I > 0$. Controller (17) together with filter (18) corresponds to ideal PID controller in series with a first order lag that is very frequent for the real controller implementation, see [2]. The real controller is specified by three gains r_P, r_D, r_I and time constant T_f for the proportional, derivative, integration actions and filtering effect, respectively. To transform the controller description into parameterized form consistent with plant model (16) the relative time variable $\bar{t}$ is introduced and (17) is multiplied by K in the same way as input u on the right-hand side of (16). Then the following controller description is obtained

$$K \frac{du(\bar{t})}{d\bar{t}} = \frac{d\bar{u}(\bar{t})}{d\bar{t}} = \rho_P \frac{de_f(\bar{t})}{d\bar{t}} + \rho_D \frac{d^2 e_f(\bar{t})}{d\bar{t}^2} + \rho_I e_f(\bar{t}) \tag{20}$$

where the gains are replaced by the dimensionless parameters as follows

$$\rho_P = K r_P, \quad \rho_D = \frac{K r_D}{\sqrt[3]{c_3}}, \quad \rho_I = K r_I \sqrt[3]{c_3} \tag{21}$$

and gain K is merged with the proportional, derivative and integration gains in (21). Then the ρ_P, ρ_D and ρ_I are the loop gains absorbing the gain K and the filter time constant is in analogy with (15) expressed in dimensionless form

$$\tau = \frac{T_f}{\sqrt[3]{c_3}} \tag{22}$$

The dimensionless plant model (16) can be expressed in the form

$$\frac{d^3 y(\bar{t})}{d\bar{t}^3} + \frac{1}{\lambda_2}\frac{d^2 y(\bar{t})}{d\bar{t}^2} + \frac{1}{\lambda_1}\frac{dy(\bar{t})}{d\bar{t}} + y(\bar{t}) = \bar{u}(\bar{t} - \vartheta) \tag{23}$$

where K is already absorbed with respect to (20). Beside the plant model (23) let be also introduced the *integrating* plant model as follows

$$\frac{d^3 y(\bar{t})}{d\bar{t}^3} + \frac{1}{\lambda_2}\frac{d^2 y(\bar{t})}{d\bar{t}^2} + \frac{1}{\lambda_1}\frac{dy(\bar{t})}{d\bar{t}} = \bar{u}(\bar{t} - \vartheta) \tag{24}$$

with considered control input (20). Without any necessity of the proof the model (24) is dimensionless model of that model type (1) where the absolute term, $y(t)$, on the left-hand side is missing. Closing the feedback loop of plant (23) or (24) and controller (20), providing also measurement and derivative action filtering, the characteristic quasi-polynomial of the loop is in the form

$$P(\bar{s}) = \tau\bar{s}^5 + \left(1 + \tau\lambda_2^{-1}\right)\bar{s}^4 + \left(\lambda_2^{-1} + \tau\lambda_1^{-1}\right)\bar{s}^3 + \left(\tau + \lambda_1^{-1} + \rho_D e^{-\vartheta\bar{s}}\right)\bar{s}^2 + \left(1 + \rho_P e^{-\vartheta\bar{s}}\right)\bar{s} + \rho_I e^{-\vartheta\bar{s}} \tag{25}$$

or

$$P(\bar{s}) = \tau\bar{s}^5 + \left(1 + \tau\lambda_2^{-1}\right)\bar{s}^4 + \left(\lambda_2^{-1} + \tau\lambda_1^{-1}\right)\bar{s}^3 + \left(\lambda_1^{-1} + \rho_D e^{-\vartheta\bar{s}}\right)\bar{s}^2 + \rho_P e^{-\vartheta\bar{s}}\bar{s} + \rho_I e^{-\vartheta\bar{s}} \tag{26}$$

respectively. In contrast to $M(\bar{s})$ the characteristic equation, $P(\bar{s}) = 0$, contains the exponential terms with the *laggardness* number ϑ and therefore has infinite spectrum of roots. This spectrum does not change if (25) or (26) is multiplied by nonzero $\exp(\vartheta\bar{s})$, $\forall\bar{s} \in C$, [52], and thus the characteristic quasi-polynomial is modified to the form

$$\left[\tau\bar{s}^5 + \left(1 + \tau\lambda_2^{-1}\right)\bar{s}^4 + \left(\lambda_2^{-1} + \tau\lambda_1^{-1}\right)\bar{s}^3 + \left(\tau + \lambda_1^{-1}\right)\bar{s}^2 + \bar{s}\right]e^{\vartheta\bar{s}} + \rho_D\bar{s}^2 + \rho_P\bar{s} + \rho_I = Q(\bar{s}) \tag{27}$$

or

$$\left[\tau\bar{s}^5 + \left(1 + \tau\lambda_2^{-1}\right)\bar{s}^4 + \left(\lambda_2^{-1} + \tau\lambda_1^{-1}\right)\bar{s}^3 + \lambda_1^{-1}\bar{s}^2\right]e^{\vartheta\bar{s}} + \rho_D\bar{s}^2 + \rho_P\bar{s} + \rho_I = Q(\bar{s}) \tag{28}$$

respectively, where the control loop gains are free of delay term.

A. ULTIMATE FREQUENCY NUMBER AND ULTIMATE LOOP GAIN ASSESSMENT

The ultimate frequency of the plant ω_K and ultimate loop gain r_K are significant parameters for tuning the controller. Consistently with the control loop model parameterization in (20) and (23) instead of ω_K the *ultimate frequency number*

$$\nu_K = \omega_K \sqrt[3]{c_3} \tag{29}$$

and ultimate loop gain $\rho_K = K r_K$ are introduced. Their values corresponding to plant model (23) are given by the following Theorem 1.

Theorem 1: Suppose the plant given by the model (23) and close a proportional feedback with the ultimate loop gain, ρ_K. The ultimate frequency number ν_K is the smallest positive solution to equation

$$\cot(\vartheta\nu_K) = \frac{1}{\nu_K} \cdot \frac{\lambda_2^{-1}\nu_K^2 - 1}{\lambda_1^{-1} - \nu_K^2} \tag{30}$$

Proof: Recall plant model (23) and close proportional feedback $\bar{u}(\bar{t}) = -\rho_P y(\bar{t})$. Characteristic equation of the loop is not algebraic any more

$$\bar{s}^3 + \lambda_2^{-1}\bar{s}^2 + \lambda_1^{-1}\bar{s} + 1 + \rho_P e^{-\vartheta\bar{s}} = 0 \tag{31}$$

For the case of ultimate oscillation at ultimate frequency given by $\nu = \nu_K$ the complex variable is $\bar{s} = j\nu_K$ and

proportional gain is ultimate $\rho_P = \rho_K$. For this case the ultimate parameters, ν_K and ρ_K, satisfy the following equality

$$(j\nu_K)^3+\lambda_2^{-1}(j\nu_K)^2+\lambda_1^{-1}j\nu_K+1 \\ +\rho_K(\cos(\vartheta\nu_K)-j\sin(\vartheta\nu_K))=0 \quad (32)$$

For real and imaginary parts of this equality the following equalities result

$$-\lambda_2^{-1}\nu_K^2+1+\rho_K\cos(\vartheta\nu_K)=0 \quad (33)$$

and

$$-\nu_K^3+\lambda_1^{-1}\nu_K-\rho_K\sin(\vartheta\nu_K)=0 \quad (34)$$

After expressing the ratio of $\cos(\vartheta\nu_K)$ and $\sin(\vartheta\nu_K)$ the relation (30) is obtained. From (33) also the ultimate loop gain results as follows

$$\rho_K=\frac{\lambda_2^{-1}\nu_K^2-1}{\cos(\vartheta\nu_K)} \quad (35)$$

The proof is finished.

How to evaluate ν_K according to (30) is shown in Sample example in Section VI.A. For integrating plants (24) the following relation for the ultimate frequency number, ν_K, is obtained

$$\cot(\vartheta\nu_K)=\frac{\lambda_2^{-1}\nu_K}{\lambda_1^{-1}-\nu_K^2} \quad (36)$$

and for the ultimate loop gain the following relation is acquired

$$\rho_K=\frac{\lambda_2^{-1}\nu_K^2}{\cos(\vartheta\nu_K)} \quad (37)$$

One can see that relations (36) and (37) are achieved directly from (30) and (35), respectively, by leaving out the stand-alone unit -1 in numerators. Additionally, in (36) the power of ν_K is cancelled due to the fact that only non-zero and smallest positive ν_K is searched.

The ultimate frequency number, ν_K, is given by the plant similarity numbers λ_1, λ_2 and the laggardness number ϑ. Its value can be displayed over an area of λ_1, λ_2 for fixed value of ϑ. For the laggardness number $\vartheta = 0.3$ its dependence on λ_1, λ_2 over the area $\lambda_1 \in \langle 0.1, 0.9\rangle$ and $\lambda_2 \in \langle 0.2, 2.4\rangle$ is plotted in Fig. 1. The intervals of λ_1, λ_2 correspond with the constraints further specified in Section III.B.

For longer delays, $\vartheta > 0.3$, the shape of the surface does not change only its level is accordingly shifted to lower ν_K values. Considering higher values of ϑ than 0.5 turns out to be unsuitable for using the dominant pole placement for tuning PID controller for plants of type (1), as it is discussed in Section V. In Fig. 2 the ultimate loop gain, ρ_K, is plotted for the same area of λ_1, λ_2 and for $\vartheta = 0.3$ as in Fig. 1.

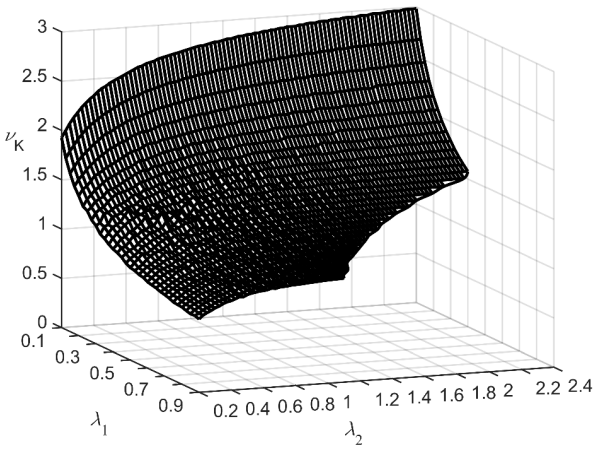

FIGURE 1. Ultimate frequency number in case of stable plants (23).

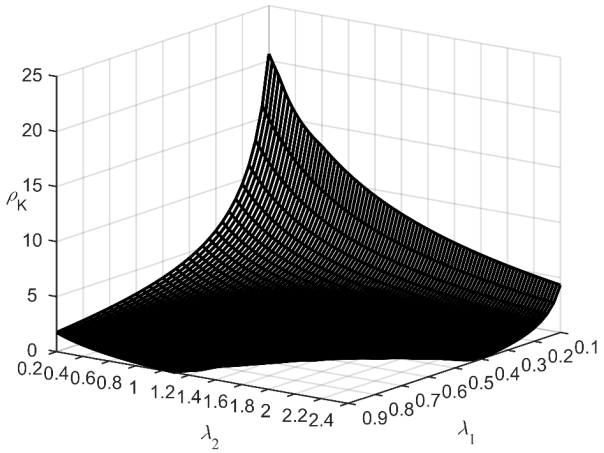

FIGURE 2. Ultimate loop gain in case of stable plants (23).

B. CONSTRAINTS ON THE CONSIDERED PLANTS

The PID control principle is not capable to cope with third order plant dynamics in their whole range. Not only unstable plants but also a part of the others is to be excluded from consideration. Some of them are quite incompatible with PID and some can be controlled by PID but their setting by means of common tuning rules does not lead to acceptable results.

The similarity numbers λ_1, λ_2 and ϑ of the plant introduced by (11) or (13) and (15) serve as generalized parameters in which the suitable range of plants can be effectively displayed. Due to generic meaning of λ_1, λ_2 and ϑ the range of acceptable plants can be expressed universally with them. The following three constraints are to be respected in the rest of the paper.

1) CONSTRAINT ON PLANT CHARACTER

Unstable plants with $\lambda_1\lambda_2 \geq 1$ and the plants approaching the *stiff-character* cases where

$$\chi, \chi_{1,2} \leq 0.05, \quad \chi, \chi_{1,2} \geq 10 \quad (38)$$

are excluded. Also, the too oscillating plants with damping $\xi < 0.05$ ($\lambda_1 > 0.9$, $\lambda_2 > 2.4$) are not considered at all. First, the plants *free of delay*, with laggardness $\vartheta = 0$, are viewed in the plane of plant similarity numbers λ_1, λ_2. Their acceptability for applying pole placement in tuning the PID loop is strongly dependent on ϑ, so that the final area of the considered λ_1, λ_2 options is considerably reduced with growing ϑ, see Section V. The mapping in Fig. 3 shows the area of λ_1, λ_2 of the delay-free plants with *laggardness* $\vartheta = 0$, for which the pole placement is applicable. Only a restricted part of this area with $\lambda_{1,2} \leq 1/3$ corresponds to *aperiodic* plants, option (4), the vast majority of the map belongs to *oscillatory* plants, option (5), with complex conjugate pair of roots. In this area the isolines of $\chi = \text{const}$ and $\xi = \text{const}$ display the ranges of ratios χ, ξ of plants admissible for consideration. Notice that the mapping in Fig. 3 holds for arbitrary natural frequency ω_n of option (5) or for arbitrary value of b for option (4).

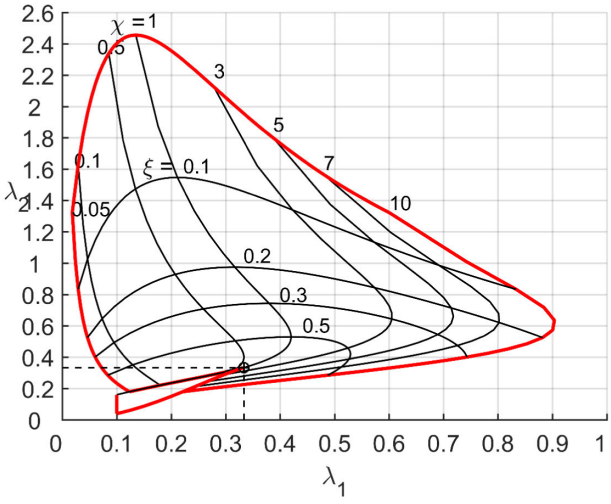

FIGURE 3. Options of λ_1, λ_2 satisfying Constraint on plant character.

2) CONSTRAINT ON PID APPLICABILITY

The applicability of PID to plant type (1) is considerably dependent on the delay, i.e. on the laggardness ϑ, and also the order of differential equation with delayed argument describing the control loop. The higher laggardness the more reduced is the admissible λ_1, λ_2 area compared with Fig. 3 which was provided for the delay-free case. This reduction involves exclusively the oscillatory plants with lower damping ratio ξ. The higher ϑ the higher lies the lower boundary of ξ. From characteristic quasi-polynomial (27) or (28) it is further apparent that the PID influences mainly the *lower derivative terms*, $\bar{s}^0, \bar{s}, \bar{s}^2$ while $\bar{s}^3, \bar{s}^4, \bar{s}^5$ are out of any influence, except for filter time constant τ. Therefore in reaching successful PID control application only plants with sufficiently low λ_2 values are applicable (the coefficient is λ_2^{-1}). In fact, the upper bound of λ_2 is considerably lower than that in Fig. 3 if $\vartheta > 0$. The higher the laggardness ϑ the lower is the upper bound of λ_2.

C. ROBUSTNESS CONSTRAINTS IMPOSED ON THE CONTROL LOOP

The robustness to the third-order plants with delay (23) or (24) is characterized by maximum sensitivities, e.g. [27],

$$M_S = \max_{\nu} |S(j\nu)|, \quad M_t = \max_{\nu} |T(j\nu)| \tag{39}$$

where

$$S(\bar{s}) = \frac{1}{1+G(\bar{s})\,C(\bar{s})} = \frac{1}{1+L(\bar{s})},$$
$$T(\bar{s}) = \frac{L(\bar{s})}{1+L(\bar{s})} \tag{40}$$

and $\bar{s} = j\nu$. Transfer functions $G(\bar{s})$ and $C(\bar{s})$ coming from Laplace transform of (23) or (24) and (20) together with (18), respectively, are given as follows

$$G(\bar{s}) = \frac{e^{-\vartheta\bar{s}}}{\bar{s}^3+\lambda_2^{-1}\bar{s}^2+\lambda_1^{-1}\bar{s}+1} \tag{41}$$

or

$$G(\bar{s}) = \frac{e^{-\vartheta\bar{s}}}{\bar{s}^3+\lambda_2^{-1}\bar{s}^2+\lambda_1^{-1}\bar{s}} \tag{42}$$

and

$$C(\bar{s}) = \frac{\rho_D\bar{s}^2+\rho_P\bar{s}+\rho_I}{\bar{s}(\tau\bar{s}+1)} \tag{43}$$

respectively. Additionally, to avoid the reference tracking degradation the prefilter due to (19) and with respect to (21) is as follows

$$F(\bar{s}) = \frac{\rho_I}{\rho_D\bar{s}^2+\rho_P\bar{s}+\rho_I} \tag{44}$$

which is used for the reference variable prefiltering in the classical control loop in Fig. 4. This control scheme also allows for the measurement noise and derivative action filtering.

Besides the maximum sensitivities, M_S and M_t, the following measure

$$M_u = \max_{\nu} |C(j\nu)\,S(j\nu)| \tag{45}$$

is to be considered, [8]. Quantity M_u characterizes high-frequency control sensitivity that in case of the PID control depends particularly on the derivative time constant ratio to the filter time constant

$$N = \frac{\rho_D}{\rho_P\tau} = \frac{\tau_D}{\tau} = \frac{T_D}{T_f} \tag{46}$$

where $\tau_D = T_D/\sqrt[3]{c_3}$. Ratio N cannot be arbitrarily large and its maximal range is between 5 and 30, see [2]. The value of N is selected from this range in dependence on measurement noise frequency range and level, for more details see [27], [29]. As regards the maximum sensitivities, M_S and M_t, their default value is 1.4 but can be ranged between 1.2 and 2, for instance [8], [53], [54]. The sensitivity function

in (40) results with respect to process transfer function (41) and controller (43) as follows

$$S(\bar{s}) = \frac{\bar{s}(\tau\bar{s}+1)\left(\bar{s}^3+\lambda_2^{-1}\bar{s}^2+\lambda_1^{-1}\bar{s}+1\right)}{\left(\begin{array}{l}\tau\bar{s}^5+\left(1+\tau\lambda_2^{-1}\right)\bar{s}^4+\left(\lambda_2^{-1}+\tau\lambda_1^{-1}\right)\bar{s}^3+\\ \left(\tau+\lambda_1^{-1}+\rho_D e^{-\vartheta\bar{s}}\right)\bar{s}^2+\left(1+\rho_P e^{-\vartheta\bar{s}}\right)\bar{s}+\rho_I e^{-\vartheta\bar{s}}\end{array}\right)} \tag{47}$$

The load disturbance supposed of the same transfer function $G(\bar{s})$ as the control variable in (2) its control loop transfer function originates in

$$\begin{aligned} &S_d(\bar{s}) \\ &= G(\bar{s})\,S(\bar{s}) = \frac{G(\bar{s})}{1+G(\bar{s})\,C(\bar{s})} = \frac{G(\bar{s})}{1+L(\bar{s})} \\ &= \frac{\bar{s}(\tau\bar{s}+1)\,e^{-\vartheta\bar{s}}}{\left(\begin{array}{l}\tau\bar{s}^5+\left(1+\tau\lambda_2^{-1}\right)\bar{s}^4+\left(\lambda_2^{-1}+\tau\lambda_1^{-1}\right)\bar{s}^3\\ +\left(\tau+\lambda_1^{-1}+\rho_D e^{-\vartheta\bar{s}}\right)\bar{s}^2+\left(1+\rho_P e^{-\vartheta\bar{s}}\right)\bar{s}+\rho_I e^{-\vartheta\bar{s}}\end{array}\right)} \end{aligned} \tag{48}$$

However, with respect to the control scheme in Fig. 4 the reference transfer function is different from the complementary sensitivity function, $T(\bar{s})$, as follows

$$T_w(\bar{s}) = T(\bar{s})\,F(\bar{s}) = \frac{G(\bar{s})\,C(\bar{s})}{1+G(\bar{s})\,C(\bar{s})}F(\bar{s}) \tag{49}$$

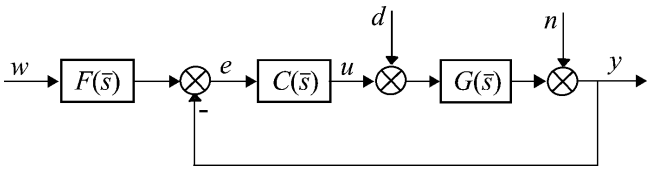

FIGURE 4. Control scheme.

After substituting for $G(\bar{s})$, $C(\bar{s})$ and $F(\bar{s})$ in (49) the reference transfer function is obtained as follows

$$\begin{aligned} &T_w(\bar{s}) \\ &= \frac{\rho_I e^{-\vartheta\bar{s}}}{\left(\begin{array}{l}\tau\bar{s}^5+\left(1+\tau\lambda_2^{-1}\right)\bar{s}^4+\left(\lambda_2^{-1}+\tau\lambda_1^{-1}\right)\bar{s}^3\\ +\left(\tau+\lambda_1^{-1}+\rho_D e^{-\vartheta\bar{s}}\right)\bar{s}^2+\left(1+\rho_P e^{-\vartheta\bar{s}}\right)\bar{s}+\rho_I e^{-\vartheta\bar{s}}\end{array}\right)} \end{aligned} \tag{50}$$

or

$$T_w(\bar{s}) = \frac{\rho_I e^{-\vartheta\bar{s}}}{\left(\begin{array}{l}\tau\bar{s}^5+\left(1+\tau\lambda_2^{-1}\right)\bar{s}^4+\left(\lambda_2^{-1}+\tau\lambda_1^{-1}\right)\bar{s}^3\\ +\left(\lambda_1^{-1}+\rho_D e^{-\vartheta\bar{s}}\right)\bar{s}^2+\rho_P e^{-\vartheta\bar{s}}\bar{s}+\rho_I e^{-\vartheta\bar{s}}\end{array}\right)} \tag{51}$$

Potential pole-zero cancellation within the delayed control loop results from the numerator in (47) where in fact only the complex conjugate poles of plant option (5) can be cancelled due to four dominant poles prescribed as two complex conjugate pairs, as proposed in Section IV. Since these pairs are prescribed to provide a well-damped disturbance rejection only such plants with $\xi > 0.4$ could be really cancelled. In addition, the range of these plants is tight as shown in Fig. 3 and controlling the well-damped processes ($\xi > 0.5$) do not represent any problem for the practice, as a rule. That is why a test benchmark process of the class of the third-order plants with delay is selected a poorly damped process with $\xi < 0.4$, see Section VI. Next, the measurement filter's pole location is far away to the left in the complex plane from a quadruple of prescribed poles, see Section IV, so that no dominant pole-zero cancellation takes place. Due to the infinite spectrum of characteristic quasi-polynomial (25) or (26) only the rightmost spectrum is eligible to possible degradation. Cancelling some of the rest of infinite spectrum, i.e. some non-dominant poles, these poles cancellation cannot be responsible for the disturbance rejection deterioration because the disturbance rejection response dynamics is characterized by the dominant pole spectrum assigned. At last, thanks the reference variable prefiltering the reference tracking is free of any pole-zero cancellation as proved by the transfer function structure in (50) or (51) and prefilter $F(\bar{s})$ results with damping factor at least 0.5 as gained by optimum values of real controller parameters in Section V.

IV. DOMINANT FOUR-POLE PLACEMENT

Characteristic equation of the loop $Q(\bar{s}) = 0$ admits an infinite spectrum of the roots, where only a little group on the rightmost positions determines the dynamic properties of the loop. The potential of four controller parameters is to adjust only four poles of the infinite spectrum as presented in Theorem 2 below. Hence if the four-pole placement technique should fulfil the assignment aim the prescribed poles have to become really dominant for the loop as presented in Theorem 3 following the Theorem 2. Particularly no other pole of the rest of the spectrum may lie *to the right* from the prescribed quadruple of poles. The more to the left from the placed poles is located the rest of the spectrum the more dominant is their position.

A. FOUR-POLE PLACEMENT TECHNIQUE

The following procedure of dominant four-pole placement is based on that in [30] where the original dominant three-pole placement introduced in [55] is adapted for filtered PID control loop. As novel feature the dominant four-pole placement is extended for the third-order plants with delay characterized by the three parameters λ_1, λ_2, ϑ of the plant model (23) or (24). Additionally, the natural frequency ratio, η, is new introduced parameter to meet the robustness requirement by its optimization. As the well-damped and robust control response the following quadruple of poles

$$\bar{p}_{1,2} = (-\delta \pm j)\,\nu, \quad \bar{p}_{3,4} = \left(-\frac{\kappa\delta}{\eta} \pm j\right)\eta\nu \tag{52}$$

where $\nu, \delta, \kappa, \eta > 0$ is prescribed to adjust the proportional, derivative, integration control loop gains ρ_P, ρ_D, ρ_I, and the filter time constant τ, respectively. The prescribed pole locations represent a well-damped and fast oscillatory behavior of control loop characterized by the damping ratio δ, the root ratio κ given by

$$\kappa = \frac{\mathrm{Re}\left(\bar{p}_{3,4}\right)}{\mathrm{Re}\left(\bar{p}_{1,2}\right)} > 0 \tag{53}$$

and the ratio between two natural frequencies given by $\eta < 1$ where the greater natural frequency is identified with the ultimate frequency, i.e. $\nu = \nu_K$. This is the rule of thumb to assign the natural frequency as the ultimate frequency which leads in practice to satisfactory disturbance rejection performance, [55], [56]. Thus, the lower natural frequency assigned is given as $\eta\nu_K$ and η is the key ratio introduced for achieving the robustness.

Theorem 2: Consider a set of third order plants characterized by the numbers λ_1, λ_2, ϑ as in (23) and close filtered PID control loop according to (20) so that the characteristic quasi-polynomial in (27) is obtained. Four complex numbers $\bar{p}_1$, $\bar{p}_2$, $\bar{p}_3$, $\bar{p}_4$ given as in (52) are selected to be placed as the dominant zeros of $Q(\bar{s})$. Without guaranteeing the (52) dominance a priori, the following setting of the control loop gains and filter time constant provides the placement of these zeros

$$\rho_P = \left(\det\begin{bmatrix} -\delta, & \delta^2-1, & 1, & A_R \\ 1, & -2\delta, & 0, & A_I \\ -\kappa\delta, & \kappa^2\delta^2-\eta^2, & 1, & A_{R\eta} \\ \eta, & -2\kappa\delta\eta, & 0, & A_{I\eta} \end{bmatrix}\right)^{-1} \times \det\begin{bmatrix} B_R, & \delta^2-1, & 1, & A_R \\ B_I, & -2\delta, & 0, & A_I \\ B_{R\eta}, & \kappa^2\delta^2-\eta^2, & 1, & A_{R\eta} \\ B_{I\eta}, & -2\kappa\delta\eta, & 0, & A_{I\eta} \end{bmatrix} \tag{54}$$

$$\rho_D = \nu^{-1}\left(\det\begin{bmatrix} -\delta, & \delta^2-1, & 1, & A_R \\ 1, & -2\delta, & 0, & A_I \\ -\kappa\delta, & \kappa^2\delta^2-\eta^2, & 1, & A_{R\eta} \\ \eta, & -2\kappa\delta\eta, & 0, & A_{I\eta} \end{bmatrix}\right)^{-1} \times \det\begin{bmatrix} -\delta, & B_R, & 1, & A_R \\ 1, & B_I, & 0, & A_I \\ -\kappa\delta, & B_{R\eta}, & 1, & A_{R\eta} \\ \eta, & B_{I\eta}, & 0, & A_{I\eta} \end{bmatrix} \tag{55}$$

$$\rho_I = \nu\left(\det\begin{bmatrix} -\delta, & \delta^2-1, & 1, & A_R \\ 1, & -2\delta, & 0, & A_I \\ -\kappa\delta, & \kappa^2\delta^2-\eta^2, & 1, & A_{R\eta} \\ \eta, & -2\kappa\delta\eta, & 0, & A_{I\eta} \end{bmatrix}\right)^{-1} \times \det\begin{bmatrix} -\delta, & \delta^2-1, & B_R, & A_R \\ 1, & -2\delta, & B_I, & A_I \\ -\kappa\delta, & \kappa^2\delta^2-\eta^2, & B_{R\eta}, & A_{R\eta} \\ \eta, & -2\kappa\delta\eta, & B_{I\eta}, & A_{I\eta} \end{bmatrix} \tag{56}$$

$$\tau = \nu^{-1}\left(\det\begin{bmatrix} -\delta, & \delta^2-1, & 1, & A_R \\ 1, & -2\delta, & 0, & A_I \\ -\kappa\delta, & \kappa^2\delta^2-\eta^2, & 1, & A_{R\eta} \\ \eta, & -2\kappa\delta\eta, & 0, & A_{I\eta} \end{bmatrix}\right)^{-1} \times \det\begin{bmatrix} -\delta, & \delta^2-1, & 1, & B_R \\ 1, & -2\delta, & 0, & B_I \\ -\kappa\delta, & \kappa^2\delta^2-\eta^2, & 1, & B_{R\eta} \\ \eta, & -2\kappa\delta\eta, & 0, & B_{I\eta} \end{bmatrix} \tag{57}$$

where the entries, $A_R, A_I, A_{R\eta}, A_{I\eta}$ and $B_R, B_I, B_{R\eta}, B_{I\eta}$, are given as follows

$$A_R = e^{-\delta\vartheta\nu}\left[a_R\cos(\vartheta\nu) - a_I\sin(\vartheta\nu)\right] \tag{58}$$
$$A_I = e^{-\delta\vartheta\nu}\left[a_I\cos(\vartheta\nu) + a_R\sin(\vartheta\nu)\right] \tag{59}$$
$$A_{R\eta} = e^{-\kappa\delta\vartheta\nu}\left[a_{R\eta}\cos(\vartheta\eta\nu) - a_{I\eta}\sin(\vartheta\eta\nu)\right] \tag{60}$$
$$A_{I\eta} = e^{-\kappa\delta\vartheta\nu}\left[a_{I\eta}\cos(\vartheta\eta\nu) + a_{R\eta}\sin(\vartheta\eta\nu)\right] \tag{61}$$

with

$$a_R = \nu^3\left(10\delta^3-\delta^5-5\delta\right) + \lambda_2^{-1}\nu^2\left(\delta^4-6\delta^2+1\right) + \lambda_1^{-1}\nu\left(3\delta-\delta^3\right) + \delta^2 - 1 \tag{62}$$

$$a_I = \nu^3\left(5\delta^2\left(\delta^2-2\right)+1\right) + \lambda_2^{-1}\nu^2 4\delta\left(1-\delta^2\right) + \lambda_1^{-1}\nu\left(3\delta^2-1\right) - 2\delta \tag{63}$$

$$a_{R\eta} = \nu^3\left(10\kappa^3\delta^3\eta^2 - \kappa^5\delta^5 - 5\kappa\delta\eta^4\right) + \lambda_2^{-1}\nu^2\left(\kappa^4\delta^4 - 6\kappa^2\delta^2\eta^2 + \eta^4\right) + \lambda_1^{-1}\nu\left(3\kappa\delta\eta^2 - \kappa^3\delta^3\right) + \kappa^2\delta^2 - \eta^2 \tag{64}$$

$$a_{I\eta} = \nu^3\left(5\kappa^2\delta^2\left(\kappa^2\delta^2\eta - 2\eta^3\right) + \eta^5\right) + \lambda_2^{-1}\nu^2 4\kappa\delta\left(\eta^3 - \kappa^2\delta^2\eta\right) + \lambda_1^{-1}\nu\left(3\kappa^2\delta^2\eta - \eta^3\right) - 2\kappa\delta\eta \tag{65}$$

and

$$B_R = e^{-\delta\vartheta\nu}\left[b_R\cos(\vartheta\nu) - b_I\sin(\vartheta\nu)\right] \tag{66}$$
$$B_I = e^{-\delta\vartheta\nu}\left[b_I\cos(\vartheta\nu) + b_R\sin(\vartheta\nu)\right] \tag{67}$$
$$B_{R\eta} = e^{-\kappa\delta\vartheta\nu}\left[b_{R\eta}\cos(\vartheta\eta\nu) - b_{I\eta}\sin(\vartheta\eta\nu)\right] \tag{68}$$
$$B_{I\eta} = e^{-\kappa\delta\vartheta\nu}\left[b_{I\eta}\cos(\vartheta\eta\nu) + b_{R\eta}\sin(\vartheta\eta\nu)\right] \tag{69}$$

and

$$b_R = \nu^3\left(-\delta^4+6\delta^2-1\right) + \lambda_2^{-1}\nu^2\left(\delta^3-3\delta\right) + \lambda_1^{-1}\nu\left(1-\delta^2\right) + \delta \tag{70}$$

$$b_I = \nu^3 4\delta\left(\delta^2-1\right) + \lambda_2^{-1}\nu^2\left(1-3\delta^2\right) + \lambda_1^{-1}2\delta\nu - 1 \tag{71}$$

$$b_{R\eta} = \nu^3\left(-\kappa^4\delta^4 + 6\kappa^2\delta^2\eta^2 - \eta^4\right) + \lambda_2^{-1}\nu^2\left(\kappa^3\delta^3 - 3\kappa\delta\eta^2\right) + \lambda_1^{-1}\nu\left(\eta^2 - \kappa^2\delta^2\right) + \kappa\delta \tag{72}$$

$$b_{I\eta} = \nu^3 4\kappa\delta\left(\kappa^2\delta^2\eta - \eta^3\right) + \lambda_2^{-1}\nu^2\left(\eta^3 - 3\kappa^2\delta^2\eta\right) + \lambda_1^{-1}\nu 2\kappa\delta\eta - \eta \tag{73}$$

respectively. Simultaneously the dominance of placed $\bar{p}_1, \bar{p}_2, \bar{p}_3, \bar{p}_4$ is checked posteriori applying Theorem 3 below.

Proof: Four poles given by (52) are to be the roots of $Q(\bar{s}) = 0$ where $Q(\bar{s})$ is given by (27). Substituting the first pole, $\bar{s} = \bar{p}_1 = (-\delta+j)\,\nu$, into this equation and separating the terms with ρ_P, ρ_D, ρ_I the following equality is obtained

$$\begin{aligned}
&\rho_D\nu^2\left(\delta^2-1-2\delta j\right)+\rho_P\nu\,(-\delta+j)+\rho_I\\
&\quad=-e^{-\delta\vartheta\nu}\left[\cos(\vartheta\nu)+j\sin(\vartheta\nu)\right]\\
&\qquad\times\begin{bmatrix}\tau\nu^5\left(10\delta^3-\delta^5-5\delta+\left(5\delta^2\left(\delta^2-2\right)+1\right)j\right)\\ +\left(1+\tau\lambda_2^{-1}\right)\nu^4\left(\delta^4-6\delta^2+1+4\delta\left(1-\delta^2\right)j\right)\\ +\left(\lambda_2^{-1}+\tau\lambda_1^{-1}\right)\nu^3\left(3\delta-\delta^3+\left(3\delta^2-1\right)j\right)\\ +\left(\tau+\lambda_1^{-1}\right)\nu^2\left(\delta^2-1-2\delta j\right)+\nu\,(-\delta+j)\end{bmatrix}
\end{aligned}\tag{74}$$

By analogous substitution $\bar{s} = \bar{p}_3 = \left(-\kappa\delta/\eta+j\right)\eta\nu = (-\kappa\delta+j\eta)\,\nu$ the following equality results

$$\begin{aligned}
&\rho_D\nu^2\left(\kappa^2\delta^2-\eta^2-2\kappa\delta\eta j\right)+\rho_P\nu\,(-\kappa\delta+j\eta)+\rho_I\\
&=-e^{-\vartheta\kappa\delta\nu}\left[\cos(\vartheta\eta\nu)+j\sin(\vartheta\eta\nu)\right]\\
&\quad\times\begin{bmatrix}\tau\nu^5\left(\begin{array}{l}10\kappa^3\delta^3\eta^2-\kappa^5\delta^5-5\kappa\delta\eta^4\\ +\left(5\kappa^2\delta^2\left(\kappa^2\delta^2\eta-2\eta^3\right)+\eta^5\right)j\end{array}\right)\\ +\left(1+\tau\lambda_2^{-1}\right)\nu^4\left(\begin{array}{l}\kappa^4\delta^4-6\kappa^2\delta^2\eta^2+\eta^4\\ +4\kappa\delta\left(\eta^3-\kappa^2\delta^2\eta\right)j\end{array}\right)\\ +\left(\lambda_2^{-1}+\tau\lambda_1^{-1}\right)\nu^3\left(3\kappa\delta\eta^2-\kappa^3\delta^3+\left(3\kappa^2\delta^2\eta-\eta^3\right)j\right)\\ +\left(\tau+\lambda_1^{-1}\right)\nu^2\left(\kappa^2\delta^2-\eta^2-2\kappa\delta\eta j\right)+\nu\,(-\kappa\delta+j\eta)\end{bmatrix}
\end{aligned}\tag{75}$$

It remains to separate the filter time constant τ in equalities (74) and (75) as follows

$$\begin{aligned}
&\rho_D\nu^2\left(\delta^2-1-2\delta j\right)+\rho_P\nu\,(-\delta+j)+\rho_I\\
&\qquad+\tau e^{-\delta\vartheta\nu}\left[\cos(\vartheta\nu)+j\sin(\vartheta\nu)\right]\\
&\qquad\times\begin{bmatrix}\nu^5\left(10\delta^3-\delta^5-5\delta+\left(5\delta^2\left(\delta^2-2\right)+1\right)j\right)\\ +\lambda_2^{-1}\nu^4\left(\delta^4-6\delta^2+1+4\delta\left(1-\delta^2\right)j\right)\\ +\lambda_1^{-1}\nu^3\left(3\delta-\delta^3+\left(3\delta^2-1\right)j\right)+\nu^2\left(\delta^2-1-2\delta j\right)\end{bmatrix}\\
&\quad=-e^{-\delta\vartheta\nu}\left[\cos(\vartheta\nu)+j\sin(\vartheta\nu)\right]\\
&\qquad\times\begin{bmatrix}\nu^4\left(\delta^4-6\delta^2+1+4\delta\left(1-\delta^2\right)j\right)\\ +\lambda_2^{-1}\nu^3\left(3\delta-\delta^3+\left(3\delta^2-1\right)j\right)\\ +\lambda_1^{-1}\nu^2\left(\delta^2-1-2\delta j\right)+\nu\,(-\delta+j)\end{bmatrix}
\end{aligned}\tag{76}$$

and

$$\begin{aligned}
&\rho_D\nu^2\left(\kappa^2\delta^2-\eta^2-2\kappa\delta\eta j\right)+\rho_P\nu\,(-\kappa\delta+j\eta)+\rho_I\\
&\qquad+\tau e^{-\vartheta\kappa\delta\nu}\left[\cos(\vartheta\eta\nu)+j\sin(\vartheta\eta\nu)\right]\\
&\qquad\times\begin{bmatrix}\nu^5\left(\begin{array}{l}10\kappa^3\delta^3\eta^2-\kappa^5\delta^5-5\kappa\delta\eta^4+\\ +\left(5\kappa^2\delta^2\left(\kappa^2\delta^2\eta-2\eta^3\right)+\eta^5\right)j\end{array}\right)\\ +\lambda_2^{-1}\nu^4\left(\begin{array}{l}\kappa^4\delta^4-6\kappa^2\delta^2\eta^2+\eta^4\\ +4\kappa\delta\left(\eta^3-\kappa^2\delta^2\eta\right)j\end{array}\right)\\ +\lambda_1^{-1}\nu^3\left(3\kappa\delta\eta^2-\kappa^3\delta^3+\left(3\kappa^2\delta^2\eta-\eta^3\right)j\right)+\\ +\nu^2\left(\kappa^2\delta^2-\eta^2-2\kappa\delta\eta j\right)\end{bmatrix}\\
&\quad=-e^{-\vartheta\kappa\delta\nu}\left[\cos(\vartheta\eta\nu)+j\sin(\vartheta\eta\nu)\right]\\
&\qquad\times\begin{bmatrix}\nu^4\left(\kappa^4\delta^4-6\kappa^2\delta^2\eta^2+\eta^4+4\kappa\delta\left(\eta^3-\kappa^2\delta^2\eta\right)j\right)\\ +\lambda_2^{-1}\nu^3\left(3\kappa\delta\eta^2-\kappa^3\delta^3+\left(3\kappa^2\delta^2\eta-\eta^3\right)j\right)\\ +\lambda_1^{-1}\nu^2\left(\kappa^2\delta^2-\eta^2-2\kappa\delta\eta j\right)+\nu\,(-\kappa\delta+j\eta)\end{bmatrix}
\end{aligned}\tag{77}$$

respectively. Dividing the equalities for real and imaginary parts of (76) and (77), and expressing them in the matrix equation form $\boldsymbol{AP} = \boldsymbol{B}$ for the vector composed of control loop gains and filter time constant

$$\mathbf{P} = \begin{bmatrix}\rho_P & \rho_D & \rho_I & \tau\end{bmatrix}^T \tag{78}$$

the following matrices, $\boldsymbol{A}$ and $\boldsymbol{B}$, are obtained

$$\begin{aligned}
\mathbf{A} &= \begin{bmatrix}-\delta\nu, & \nu^2\left(\delta^2-1\right), & 1, & \nu^2A_R\\ \nu, & -2\delta\nu^2, & 0, & \nu^2A_I\\ -\kappa\delta\nu, & \nu^2\left(\kappa^2\delta^2-\eta^2\right), & 1, & \nu^2A_{R\eta}\\ \eta\nu, & -2\kappa\delta\eta\nu^2, & 0, & \nu^2A_{I\eta}\end{bmatrix},\\
\mathbf{B} &= \nu\begin{bmatrix}B_R\\ B_I\\ B_{R\eta}\\ B_{I\eta}\end{bmatrix}
\end{aligned}\tag{79}$$

where in case of matrix $\boldsymbol{A}$ entries

$$A_R\nu^2 = e^{-\delta\vartheta\nu}\left[a_R\cos(\vartheta\nu)-a_I\sin(\vartheta\nu)\right] \tag{80}$$
$$A_I\nu^2 = e^{-\delta\vartheta\nu}\left[a_I\cos(\vartheta\nu)+a_R\sin(\vartheta\nu)\right] \tag{81}$$
$$A_{R\eta}\nu^2 = e^{-\kappa\delta\vartheta\nu}\left[a_{R\eta}\cos(\vartheta\eta\nu)-a_{I\eta}\sin(\vartheta\eta\nu)\right] \tag{82}$$
$$A_{I\eta}\nu^2 = e^{-\kappa\delta\vartheta\nu}\left[a_{I\eta}\cos(\vartheta\eta\nu)+a_{R\eta}\sin(\vartheta\eta\nu)\right] \tag{83}$$

with

$$a_R = \nu^2\begin{bmatrix}\nu^3\left(10\delta^3-\delta^5-5\delta\right)+\lambda_2^{-1}\nu^2\left(\delta^4-6\delta^2+1\right)\\ +\lambda_1^{-1}\nu\left(3\delta-\delta^3\right)+\delta^2-1\end{bmatrix} \tag{84}$$

$$a_I = \nu^2\begin{bmatrix}\nu^3\left(5\delta^2\left(\delta^2-2\right)+1\right)+\lambda_2^{-1}\nu^2 4\delta\left(1-\delta^2\right)\\ +\lambda_1^{-1}\nu\left(3\delta^2-1\right)-2\delta\end{bmatrix} \tag{85}$$

$$a_{R\eta} = \nu^2\begin{bmatrix}\nu^3\left(10\kappa^3\delta^3\eta^2-\kappa^5\delta^5-5\kappa\delta\eta^4\right)\\ +\lambda_2^{-1}\nu^2\left(\kappa^4\delta^4-6\kappa^2\delta^2\eta^2+\eta^4\right)\\ +\lambda_1^{-1}\nu\left(3\kappa\delta\eta^2-\kappa^3\delta^3\right)+\kappa^2\delta^2-\eta^2\end{bmatrix} \tag{86}$$

$$a_{I\eta} = \nu^2\begin{bmatrix}\nu^3\left(5\kappa^2\delta^2\left(\kappa^2\delta^2\eta-2\eta^3\right)+\eta^5\right)\\ +\lambda_2^{-1}\nu^2 4\kappa\delta\left(\eta^3-\kappa^2\delta^2\eta\right)\\ +\lambda_1^{-1}\nu\left(3\kappa^2\delta^2\eta-\eta^3\right)-2\kappa\delta\eta\end{bmatrix} \tag{87}$$

and in case of matrix $\boldsymbol{B}$ entries

$$B_R\nu = e^{-\delta\vartheta\nu}\left[b_R\cos(\vartheta\nu)-b_I\sin(\vartheta\nu)\right] \tag{88}$$
$$B_I\nu = e^{-\delta\vartheta\nu}\left[b_I\cos(\vartheta\nu)+b_R\sin(\vartheta\nu)\right] \tag{89}$$
$$B_{R\eta}\nu = e^{-\kappa\delta\vartheta\nu}\left[b_{R\eta}\cos(\vartheta\eta\nu)-b_{I\eta}\sin(\vartheta\eta\nu)\right] \tag{90}$$
$$B_{I\eta}\nu = e^{-\kappa\delta\vartheta\nu}\left[b_{I\eta}\cos(\vartheta\eta\nu)+b_{R\eta}\sin(\vartheta\eta\nu)\right] \tag{91}$$

with

$$b_R = \nu\begin{bmatrix}\nu^3\left(-\delta^4+6\delta^2-1\right)+\lambda_2^{-1}\nu^2\left(\delta^3-3\delta\right)\\ +\lambda_1^{-1}\nu\left(1-\delta^2\right)+\delta\end{bmatrix} \tag{92}$$

$$b_I = \nu\left[\nu^3 4\delta\left(\delta^2-1\right)+\lambda_2^{-1}\nu^2\left(1-3\delta^2\right)+\lambda_1^{-1}2\delta\nu-1\right] \tag{93}$$

$$b_{R\eta} = \nu \begin{bmatrix} \nu^3\left(-\kappa^4\delta^4+6\kappa^2\delta^2\eta^2-\eta^4\right) \\ +\lambda_2^{-1}\nu^2\left(\kappa^3\delta^3-3\kappa\delta\eta^2\right) \\ +\lambda_1^{-1}\nu\left(\eta^2-\kappa^2\delta^2\right)+\kappa\delta \end{bmatrix} \quad (94)$$

$$b_{I\eta} = \nu \begin{bmatrix} \nu^3 4\kappa\delta\left(\kappa^2\delta^2\eta-\eta^3\right)+\lambda_2^{-1}\nu^2\left(\eta^3-3\kappa^2\delta^2\eta\right) \\ +\lambda_1^{-1}\nu 2\kappa\delta\eta-\eta \end{bmatrix} \quad (95)$$

Now from equation $\boldsymbol{AP} = \boldsymbol{B}$ the matrix solution $\boldsymbol{P} = \boldsymbol{A}^{-1}\boldsymbol{B}$ leads to the following results

$$\rho_P = \frac{\det(\mathbf{A}_P)}{\det(\mathbf{A})}, \quad \rho_D = \frac{\det(\mathbf{A}_D)}{\det(\mathbf{A})},$$
$$\rho_I = \frac{\det(\mathbf{A}_I)}{\det(\mathbf{A})}, \quad \tau = \frac{\det(\mathbf{A}_\tau)}{\det(\mathbf{A})} \quad (96)$$

where

$$\mathbf{A}_P = \begin{bmatrix} \nu B_R, & \nu^2\left(\delta^2-1\right), & 1, & \nu^2 A_R \\ \nu B_I, & -2\delta\nu^2, & 0, & \nu^2 A_I \\ \nu B_{R\eta}, & \nu^2\left(\kappa^2\delta^2-\eta^2\right), & 1, & \nu^2 A_{R\eta} \\ \nu B_{I\eta}, & -2\kappa\delta\eta\nu^2, & 0, & \nu^2 A_{I\eta} \end{bmatrix},$$

$$\mathbf{A}_D = \begin{bmatrix} -\delta\nu, & \nu B_R, & 1, & \nu^2 A_R \\ \nu, & \nu B_I, & 0, & \nu^2 A_I \\ -\kappa\delta\nu, & \nu B_{R\eta}, & 1, & \nu^2 A_{R\eta} \\ \eta\nu, & \nu B_{I\eta}, & 0, & \nu^2 A_{I\eta} \end{bmatrix},$$

$$\mathbf{A}_I = \begin{bmatrix} -\delta\nu, & \nu^2\left(\delta^2-1\right), & \nu B_R, & \nu^2 A_R \\ \nu, & -2\delta\nu^2, & \nu B_I, & \nu^2 A_I \\ -\kappa\delta\nu, & \nu^2\left(\kappa^2\delta^2-\eta^2\right), & \nu B_{R\eta}, & \nu^2 A_{R\eta} \\ \eta\nu, & -2\kappa\delta\eta\nu^2, & \nu B_{I\eta}, & \nu^2 A_{I\eta} \end{bmatrix},$$

$$\mathbf{A}_\tau = \begin{bmatrix} -\delta\nu, & \nu^2\left(\delta^2-1\right), & 1, & \nu B_R \\ \nu, & -2\delta\nu^2, & 0, & \nu B_I \\ -\kappa\delta\nu, & \nu^2\left(\kappa^2\delta^2-\eta^2\right), & 1, & \nu B_{R\eta} \\ \eta\nu, & -2\kappa\delta\eta\nu^2, & 0, & \nu B_{I\eta} \end{bmatrix} \quad (97)$$

and

$$\det(\mathbf{A}) = \nu^5 \begin{pmatrix} (\kappa-1)^2\delta^2\left(\eta A_I+A_{I\eta}\right)- \\ -2\eta\delta\left(\kappa-1\right)\left(A_R-A_{R\eta}\right)+ \\ +\left(\eta^2-1\right)\left(\eta A_I-A_{I\eta}\right) \end{pmatrix} \quad (98)$$

Matrix $\boldsymbol{A}$ is non-singular, i.e. $\det(\boldsymbol{A}) \neq 0$, if at least one of the ratios η, κ is not equal to one and $\nu > 0$, as apparent from (98). Let be remarked that for $\eta = \kappa = 1$ the relations for A_R and A_I are identical with $A_{R\eta}$ and $A_{I\eta}$, respectively. From the ratios of determinants (96) the relationships (54), (55), (56), and (57) result wherein the number ν is cancelled either partly or completely. The resulting setting is proved on the four poles dominance as presented in Theorem 3 below. The proof is finished.

Remark 1: For integrating plants (24) the relations for proportional, derivative, integration loop gains and filter time constant given by (54) through (57) are also applicable but with moderate changes in both the coefficient matrix $\boldsymbol{A}$ and the right-hand side matrix $\boldsymbol{B}$. These changes are such that in (62) and (64) last term δ^2-1 and $\kappa^2\delta^2-\eta^2$, respectively, and in (63) and (65) last term -2δ and $-2\kappa\delta\eta$, respectively, are missing. In case of $\boldsymbol{B}$ in (70) and (72) the stand-alone δ and $\kappa\delta$, respectively, and in (71) and (73) the numbers -1 and $-\eta$, respectively, are missing.

B. DOMINANCE PROOF OF THE FOUR PLACED POLES

The four pole placement according to Theorem 2 does not guarantee a priori the dominance of $\bar{p}_1$, $\bar{p}_2$, $\bar{p}_3$, $\bar{p}_4$ in $Q(\bar{s})$ infinite spectrum and therefore this dominance is to be proved before accepting the results in (54) through (57). This proof is provided by the following theorem.

Theorem 3: Consider the characteristic quasi-polynomial of the fifth-order PID control loop in the form, $P(\bar{s})$, given by (25) or (26) and suppose a straight line $\bar{s} = -\beta_m + j\omega$ for either $\beta_m > \beta = \kappa\delta\nu$, $\kappa > 1$, or $\beta_m > \beta = \delta\nu$, $\kappa < 1$, where ω is growing from zero to infinity, $\omega \to \infty$. If the following limit is reached

$$\lim_{\omega\to\infty} \arg P(\bar{s})|_{\bar{s}=-\beta_m+j\omega} - \arg P(\bar{s})|_{\bar{s}=-\beta_m} = -3\frac{\pi}{2} \quad (99)$$

then the whole rest of $P(\bar{s})$ spectrum lies to the left from the placed quadruple of poles, $\bar{p}_{1,2,3,4}$.

Proof: Consider a Jordan curve composed of the circle $\mathcal{C}$, $\bar{s} = R\left(\cos(\psi)+j\sin(\psi)\right)$, $\psi \in \langle -\pi/2-\gamma, \pi/2+\gamma\rangle$, and the straight line $\mathcal{L}$, $\bar{s} = -\beta_m+j\omega$, $\omega \in \langle -R\cos(\gamma), R\cos(\gamma)\rangle$, Fig. 5, and suppose that only *four zeros* $\bar{p}_{1,2,3,4}$ of quasi-polynomial $P(\bar{s})$ lie inside this curve.

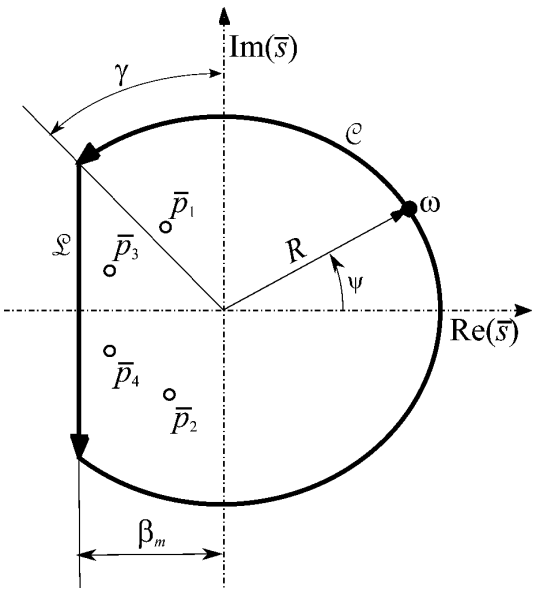

FIGURE 5. Jordan curve closed with the straight line for evaluating $\bar{p}_{1,2,3,4}$ dominance.

By the argument increment rule the total argument increment along this curve run in the clockwise direction ($\mathcal{L}$ is oriented downwards) is then 8π. This increment is composed of two increments

$$\Delta\arg_C + \Delta\arg_L = 8\pi \quad (100)$$

obtained for the parts $\mathcal{C}$ and $\mathcal{L}$, respectively. The argument increment $\Delta\arg_C$ is given by the order five of $P(\bar{s})$ and for the limit of $R \to \infty$ and $\gamma \to 0$ its value is

$$\Delta\arg_C = 5\pi \quad (101)$$

Finally realize that in (99) only *one half* of the straight line $\mathcal{L}$, which is with $\omega \geq 0$ and oriented upwards, is considered so that only $\Delta \arg_L / 2$ is to be obtained with opposite sign. Hence by comparing (100) and (101) and dividing by two the argument increment (99) is obtained, and the Theorem 3 is proved.

Let be noted that the application of rule (99) is as follows. For a constant $\beta_m > \beta = \max(\delta\nu, \kappa\delta\nu)$ quasi-polynomial function $P(-\beta_m + j\omega)$ is computed for ω from $\omega = 0$ to an enough high $\omega = \omega_m$, which renders the other terms of the quasi-polynomial negligibly small compared to ω^5. To obtain the values of $\arg P$ from a hodograph inside the unit circle of complex plane the following mapping is applied

$$\tilde{P}(\bar{s}) = \frac{P(\bar{s})}{1+|P(\bar{s})|}, \quad \bar{s} = -\beta_m + j\omega, \ \omega \in \langle 0, \omega_m \rangle \quad (102)$$

where the denominator is real and cannot change the argument value of $P(\bar{s})$. The greater ratio β_m / β for which condition (99) is satisfied the stronger is the dominance of $\bar{p}_{1,2,3,4}$. To evaluate the four-pole dominance degree the *dominance index* from [55] is modified as follows

$$\sigma = \begin{cases} \dfrac{\mathrm{Re}(\bar{p}_5)}{\mathrm{Re}(\bar{p}_{1,2})} > 1, & \kappa < 1 \\ \dfrac{\mathrm{Re}(\bar{p}_5)}{\mathrm{Re}(\bar{p}_{3,4})} > 1, & \kappa \geq 1 \end{cases} \quad (103)$$

where $\bar{p}_5$ is the rightmost pole from the rest of the $P(\bar{s})$ spectrum. This pole results in complex pole for $\kappa < 1$ while $\kappa \geq 1$ the fifth pole is real, as a rule. The effect of non-dominant poles on control loop dynamics is negligible if the non-dominant pole spectrum is separated from that dominant spectrum, [57]. Thus, a distinct separation of $\bar{p}_{1,2}$, $\bar{p}_{3,4}$ and $\bar{p}_5$ all together from the rest of the infinite spectrum is desirable for a marked dominance of them.

Remark 2: Three gains ρ_P, ρ_D, ρ_I and time constant τ according to relation (54) through (57) are derived for considered plant model (1) with the premise of prescribed poles dominance. The matrix formulae in these relations originate from the characteristic quasi-polynomial, $Q(\bar{s})$, evaluated for prescribed poles. It also includes the delay operator, $\exp(-\tau s)$, evaluation. Once poles to be prescribed are found at optimum with respect to IAE criterion and maximum sensitivities constraint the dominant pole placement is guaranteed as proved by the argument increment principle due to (99). The compactness of the controller parameter relations would be then lost if instead of all the matrix formulae their determinant evaluations are provided in fact.

V. CONTROL LOOP OPTIMIZATION IN PLANT PARAMETER SPACE

The four-pole placement parameters ν, δ, κ, η are subject to the constrained IAE optimization in the space of plant parameters λ_1, λ_2, and ϑ. Due to close relation between the ultimate frequency of the plant (23) or (24) and a desirable natural frequency of the control loop the prescription of ν value in quadruple $\bar{p}_{1,2,3,4}$ is identified due to the ultimate frequency number, ν_K, as a reference parameter of the plant. Next, the crucial constraint of the IAE criterion is the maximum sensitivity M_S limited to 1.8 as revealed within the control design for benchmark plant in Section VI. This constraint, $M_S \leq 1.8$, is not peculiar only to the benchmark plant but it is also found suitable for all considered plants characterized by numbers λ_1, λ_2, and ϑ. Beside the constraint on M_S also the constraint on the ratio N is assumed such that $5 < N < 15$ thus $N \approx 10$. Only under meeting both constraints the IAE value is minimized. This value is computed from the *load disturbance rejection* response of the loop that is frequently optimized in practice. Its loop transfer function is obtained in (48). Analogously for the integrating plants given by (24) the corresponding $S_d(\bar{s})$ is obtained when (42) is substituted for $G(\bar{s})$ in (48). The load disturbance rejection is optimized according to the IAE criterion (as also preferred in [10])

$$J = \int_0^t |e(\theta)| \, d\theta \quad (104)$$

As shown in [58], [59], the unconstrained IAE minimization leads to prescribing the natural frequency *higher* than the plant ultimate frequency. In the assessment according to Theorem 2 the relationship $\boldsymbol{P} = \boldsymbol{A}^{-1}\boldsymbol{B}$, (96), provides a mapping of the controller parameters $\boldsymbol{P} = \begin{bmatrix} \rho_P & \rho_D & \rho_I & \tau \end{bmatrix}^T$ in the space of the root coordinates ν, δ, κ, η where primarily the constrained optimization of δ, κ, η is performed. From constraining the IAE optimization it turns out that the natural frequency number should not be prescribed *higher* than the ultimate one, thus $\nu \leq \nu_K$.

The constrained IAE optimization of the control loop is performed for three parameters, ratios δ, κ, η when the natural frequency number ν is fixed to ν_K. This optimization is repeated throughout an area of plant parameters λ_1, λ_2, ϑ fulfilling the constraints on the plant character, the PID applicability and robustness, see Sections III.B and III.C. The explicit form of the pole placement relationships (54) through (57) from Section IV, makes it possible to map the control loop gains ρ_P, ρ_D, ρ_I and filter time constant τ subject to plant parameters λ_1, λ_2, ϑ and optimized ratios δ, κ, η. The optimization results are displayed in the plane of similarity numbers λ_1, λ_2 and the laggardness number ϑ is considered as a stepwise given parameter. The ultimate frequency number assigned is recorded in Fig. 1 and corresponding ultimate loop gain in Fig. 2 for $\vartheta = 0.3$. The λ_1, λ_2 area of the maps for ρ_P, ρ_D, ρ_I, τ in Figs. 6, 7, 8, 9 is considerably smaller than that given in Fig. 3 which holds for delay-free plants, $\vartheta = 0$.

For nonzero laggardness, $\vartheta > 0$, this area is strongly reduced into the admissible values of λ_1, λ_2 at which the afore mentioned constraints are satisfied by the controller parameter settings mapped. Constraining the controller tuning to $M_S \leq 1.8$ and $N \leq 10$(or 15) this tuning results in positive values of the controller parameters as a rule. Also, the varying delay effect is shown in Figs. 6-8 considering both $\vartheta = 0.3$ and $\vartheta = 0.5$. Since both surfaces on area λ_1, λ_2 are intersected in case of filter time constant τ only the surface for $\vartheta = 0.3$ is displayed in Fig. 9.

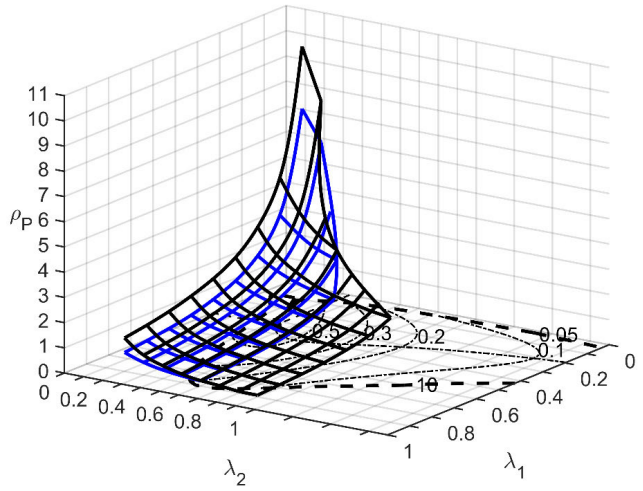

FIGURE 6. The proportional loop gain in area of $\lambda_{1,2}$ reduced from Fig. 3 in case of laggardness numbers $\vartheta = 0.3$ (black) and $\vartheta = 0.5$ (blue).

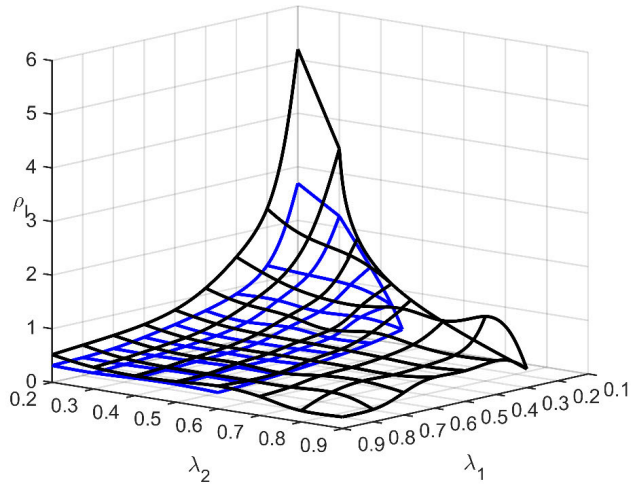

FIGURE 8. The integration loop gain in delay cases of $\vartheta = 0.3$ (black) and $\vartheta = 0.5$ (blue).

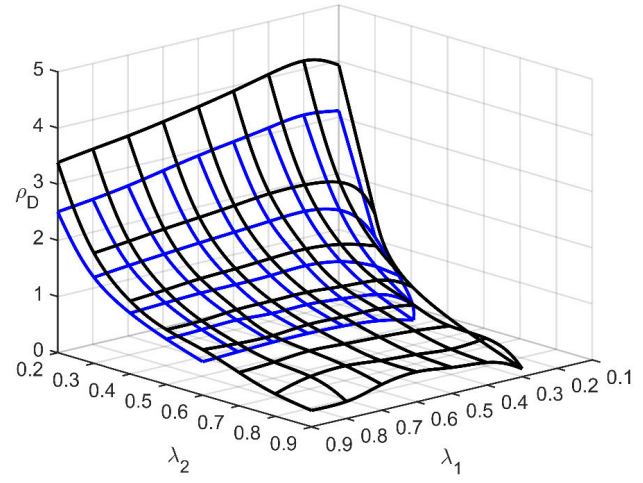

FIGURE 7. The derivative loop gain in delay cases of $\vartheta = 0.3$ (black) and $\vartheta = 0.5$ (blue).

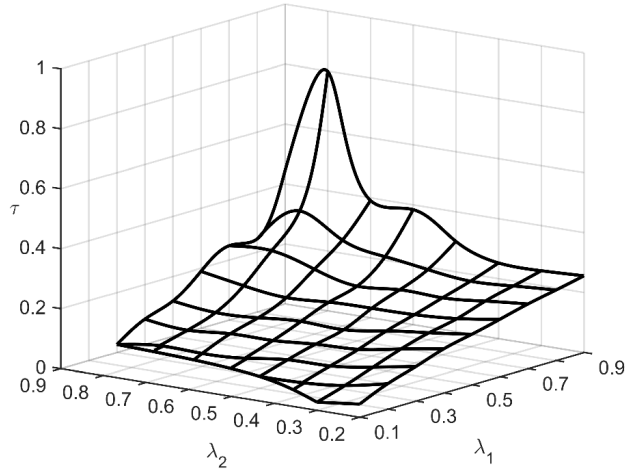

FIGURE 9. The filter time constant in case of $\vartheta = 0.3$.

The maps of M_S and N prove keeping both measures within the given constraints depicted in Fig. 10 and 11, respectively, and in Fig. 12 the resulting IAE is drawn. Particularly the range of λ_2 is considerably reduced in the part of weakly damped oscillatory plants so that only $\xi > 0.3$ is admissible, in fact, see Fig. 6. The maps for higher ϑ are of very similar shape but shifted down and with more reduced area of λ_1, λ_2. The higher ϑ the lower are the control loop gains. On the whole area the plants with laggardness number $\vartheta > 0.5$ are reduced any further when the suitability area of λ_1, λ_2 for the PID application is too limited to be mapped. For each of the pole placements according to (54) through (57) the dominance of $\bar{p}_1, \bar{p}_2, \bar{p}_3, \bar{p}_4$ is to be checked. To display this check the dominance index σ, (103), is evaluated over the whole λ_1, λ_2 area and plotted in Fig. 13, where the quadruple dominance for the plants with $\vartheta = 0.3$ is verified. This check is also verified in case of $\vartheta = 0.5$ but not displayed. However, for plants with $\vartheta = 0.5$ and $\lambda_2 > 0.6$ irrespective λ_1 value this dominance is already lost originating in the control loop instability for more oscillatory plants any further ($\xi < 0.3$). Rising the delay effect any further, $\vartheta > 0.5$, both the quadruple dominance is lost and the delayed control loop becomes unstable for plants with $\lambda_2 > 0.5$.

Near-to dominant pole-zero cancellation can appear when the quadruple dominance is lost. Then, however, the cancellation happens between the not prescribed poles and the zeros originating from poorly damped plant spectrum. Hence as $\xi \to 0$ the more the unprescribed rightmost poles are close to the stability margin and this cancellation is more plausible. Let be noted that considering only the suitable constraints and plant parameter ranges the quadruple dominance loss is avoided by the controller setting due to (54) through (57). Out of these constraints and ranges the dominant four-pole placement is not applicable to real PID tuning. Regarding the non-dominant pole spectrum separation from that rightmost spectrum this separation commonly results large enough for plants with $\vartheta \leq 0.5$ and $\xi > 0.3$ as proved in Fig. 13 and Sample example below.

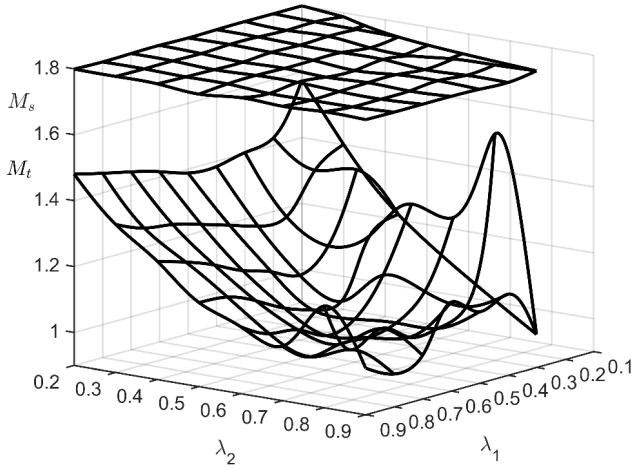

FIGURE 10. Maximum sensitivities M_S and M_t in case of $\vartheta = 0.3$.

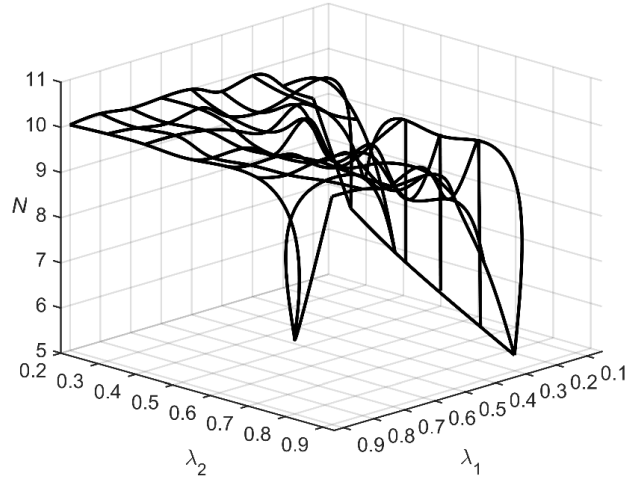

FIGURE 11. Filter's ratio N in case of $\vartheta = 0.3$.

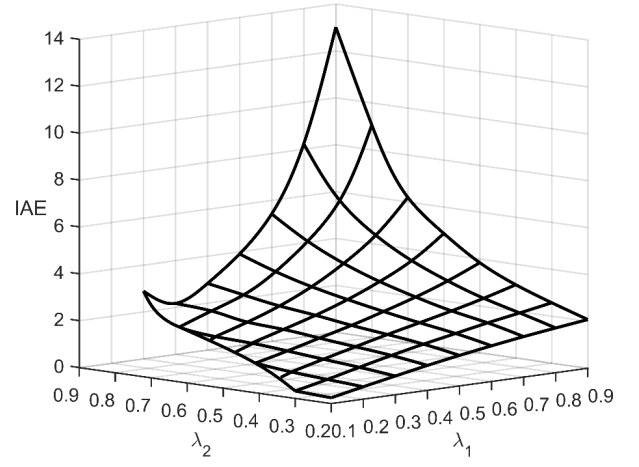

FIGURE 12. The IAE versus λ_1, λ_2 in case of $\vartheta = 0.3$.

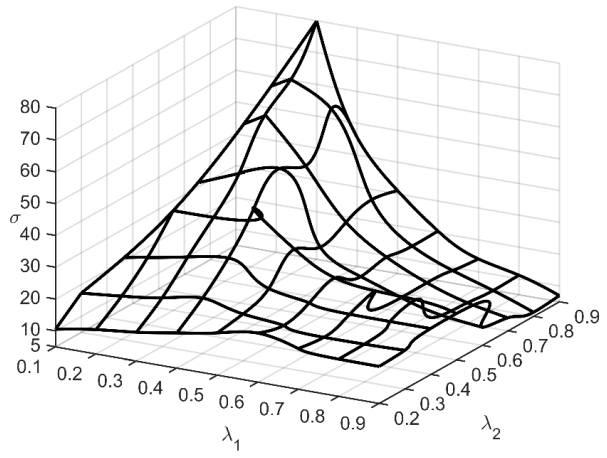

FIGURE 13. The dominance index in case of $\vartheta = 0.3$.

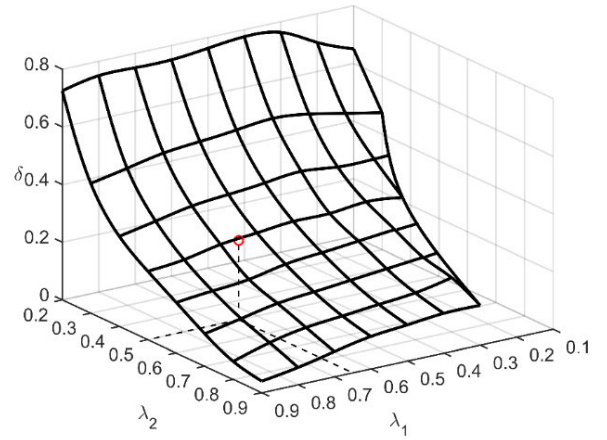

FIGURE 14. Optimum relative damping δ in case of $\vartheta = 0.3$.

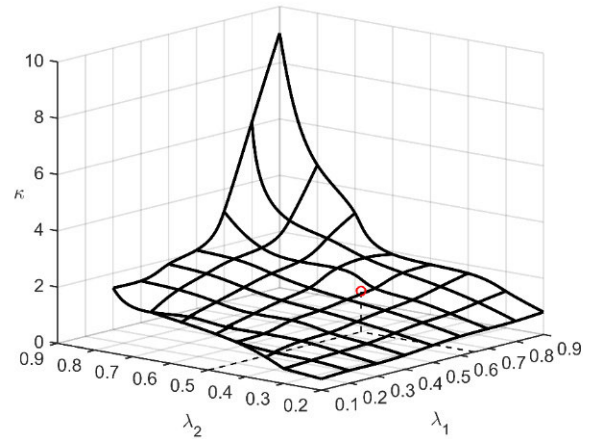

FIGURE 15. Optimum root ratio κ in case of $\vartheta = 0.3$.

The maps with optimum values of ratios δ, κ, η are presented in Figs. 14, 15 and 16, respectively, for $\vartheta = 0.3$. The higher values of λ_2 the less results $\delta \in (0.04, 0.8)$ and reversely the greater results $\kappa \in (0.4, 9)$. Regarding the new ratio η an average value across all the considered plants results in 0.35. Due to the delay effect, displayed in range $0 < \vartheta \leq 0.5$, and poor plant damping (higher values of λ_2) the maps also show boundaries in the space of similarity numbers λ_1, λ_2, ϑ wherein PID type control is still acceptable, i.e. real controller gain magnitudes are not negligible

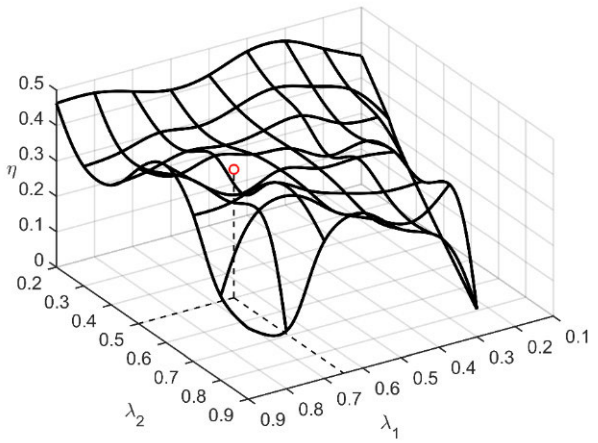

FIGURE 16. Optimum natural frequency ratio η in case of $\vartheta = 0.3$.

(there is still certain amplification at least $\rho_P \approx 0.5\rho_K$) and the filter time constant is in proper ratio to the derivative time constant. Only for a limited set of plants characterized with $\lambda_1 \leq 0.2$, $\lambda_2 > 0.4$ this ratio results $N < 5$ under keeping robustness constraint $M_S \leq 1.8$ so that PI type control takes place instead. This limited set of plants is eliminated from the maps recorded. Also the dominance index does not result so strong in this limited plant set, i.e. $\sigma \in (2, 5)$, nonetheless the dominant four-pole placement is guaranteed. All these optimum values and properties are also observed in delay case of $\vartheta = 0.5$. The plants characterized with $\lambda_1 > 0.9$, $0.4 < \lambda_2 \leq 0.6$ and $\vartheta > 0.5$ lead to poor amplification due to $\rho_P < 10^{-2}$, hence these plant options are omitted. Be assured that for $\vartheta > 0.5$ and $\lambda_2 > 0.6$ irrespective λ_1 value not only the dominance of four-pole placement is not achieved but also the delayed control loop becomes even unstable.

The proposed controller tuning procedure is summarized as follows:

1. Determine controlled plant parameters λ_1, λ_2 and ϑ due to Section II.
2. Design (adjust) maximum sensitivities $M_S(M_t)$ and/or $M_u(N)$.
3. Prescribe natural frequency $\nu = \nu_K$ and optimize ratios δ, κ, η by minimizing criterion (104) with respect to point 2.
4. Compute the real controller parameters by relations (54) through (57).
5. Evaluate the dimensional gains r_P, r_D, r_I and time constant T_f in (21) and (22), respectively, based on the knowledge of the dimensionless ones from point 4. Then the PID controller with the measurement noise filter is tuned for (industrial) application.

The IAE optimum setting within λ_1, λ_2 and ϑ boundaries for the dominant four-pole placement applicability provides competitive disturbance rejection performance due to the natural frequency assignment identical with the ultimate one and properly optimized ratios δ, κ, η. Simultaneously the reference tracking performance is not degraded by this setting as presented in Comparative study below.

VI. COMPARATIVE STUDY FOR BENCHMARK OSCILLATORY MODEL

A comparative study is demonstrated on the load disturbance rejection and reference tracking for the real controller (43) tunings based on the proposed dominant four-pole placement, lambda tuning method from [35], Åström-Hägglund tuning method, and gain and phase margin optimization method. All these tuning methods are developed for particular third-order plant with delay, except the Åström-Hägglund and gain and phase margin methods applicable to plants of arbitrary order in general. The latter method for higher-order processes achieves the phase margin up to 80°, [60]. Particularly the other tuning methods for comparison are selected due to their suitability for poorly damped processes. In this section all the considered methods are optimized for the load disturbance rejection and also tested on reference tracking capability within the control scheme in Fig. 4. As a structurally crucial benchmark model is chosen that model (23) describing the set of oscillatory plants with given similarity numbers λ_1, λ_2 and ϑ, see Sample example below.

A. SAMPLE EXAMPLE–OSCILLATORY PLANT WITH SIGNIFICANT TIME DELAY

To demonstrate the application of the above introduced dominant four-pole placement the following sample example of poorly damped oscillatory third-order plant with delay (falling into the admissible area of similarity numbers in Fig. 6)

$$8\frac{d^3y(t)}{dt^3}+8\frac{d^2y(t)}{dt^2}+3.077\,\frac{dy(t)}{dt}+y(t) = 0.8\,u(t-0.6) \quad (105)$$

is used. The original parameters of this plant option, (5), are *dimensional* as follows, $\omega_n = 0.42\ [s^{-1}]$, $\xi = 0.349$, $\chi = 4.8$, $\upsilon = 0.6\ [s]$, and from (13) and (15) the following similarity numbers result

$$\lambda_1 = 0.65, \quad \lambda_2 = 0.5, \ \vartheta = 0.3 \quad (106)$$

where the scaling factor $\sqrt[3]{c_3} = \sqrt[3]{8} = 2\ [s]$ is applied. From this parameterization the following dimensionless form (23) of the plant model is obtained

$$\frac{d^3y(\bar{t})}{d\bar{t}^3}+2\frac{d^2y(\bar{t})}{d\bar{t}^2}+1.5385\frac{dy(\bar{t})}{d\bar{t}}+y(\bar{t}) = \bar{u}(\bar{t}-0.3) \quad (107)$$

As in (23) this plant model is considered with the steady-state gain, given as $K = 0.8$, being the part of the loop gains as defined in (21). The ultimate parameters of this plant are obtained from solving (30) and (35). The solution to (30) is facilitated that, first, $\vartheta\nu_K = \Phi_K$ is calculated and then it is got back $\nu_K = \Phi_K/\vartheta$ where Φ_K is the ultimate angle. The ultimate frequency number and the ultimate loop gain are obtained as follows

$$\nu_K = 1.068, \quad \rho_K = 1.3496 \quad (108)$$

To prescribe an adequate natural frequency of the loop the value of ν is identified with ν_K from Fig. 1. To prescribe optimum dominant poles the constrained IAE optimization is performed with respect to δ, κ, and η as shown

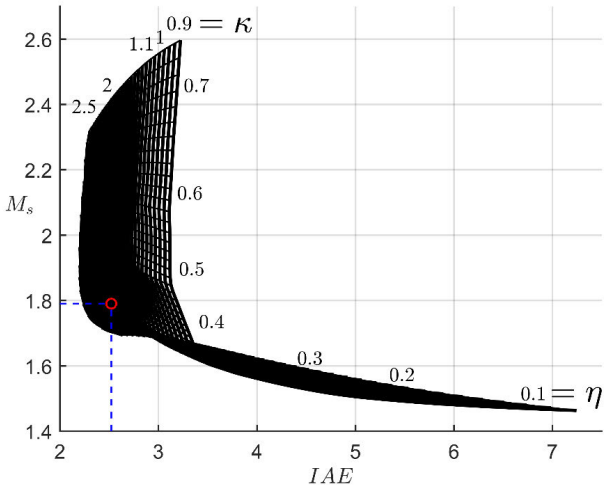

FIGURE 17. M_S versus IAE with respect to variable κ, η under optimum $\delta = 0.275$.

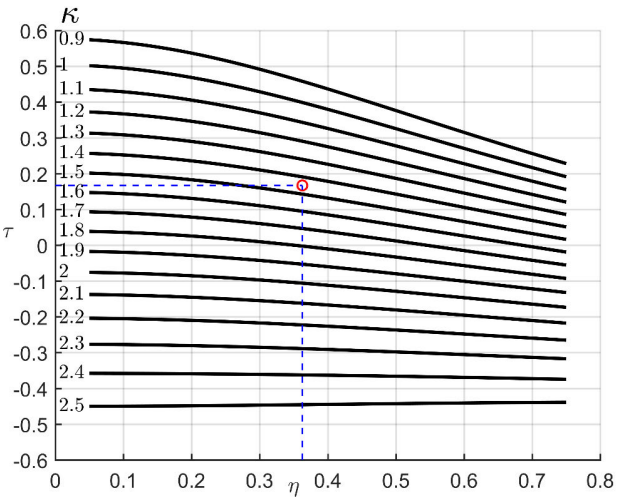

FIGURE 18. Filter time constant τ versus η with respect to stepwise κ and optimum $\delta = 0.275$.

in Fig. 17 and 18. From Fig. 17 the IAE value results in 2.5223 for $M_S \leq 1.8$ and from Fig. 18 the proper filter time constant satisfying constraint $N \leq 10$ upon optimum ratios $\delta = 0.275$, $\kappa = 1.45$ and $\eta = 0.3625$. For computing the control loop gains and filter time constant ρ_P, ρ_D, ρ_I and τ, respectively, the following quadruple of poles is prescribed

$$\bar{p}_{1,2} = -0.2936 \pm j1.068, \quad \bar{p}_{3,4} = -0.4258 \pm j0.3871 \quad (109)$$

to be used in (54) through (57). From this prescription the following control loop gains and time constant result

$$\rho_P = 0.6215,\ \rho_D = 1.0134,\ \rho_I = 0.4643,\ \tau = 0.167 \quad (110)$$

where the proportional loop gain results as $\rho_P = 0.46\rho_K \approx 0.5\rho_K$. As regards the filter's ratio (46) it originates in $N = 9.77$. Next, the maximum sensitivities, M_S and M_t, are obtained as 1.79 and 1.09, respectively. In the same way as for the plants with similarity numbers (106) the constrained IAE optimization is performed for the rest of plants (23) as shown in the maps for optimum δ, κ and η in Figs. 14, 15 and 16, respectively, where the pole placement ratios belonging to plant (107) can be found in the point $\left[\lambda_1\ \lambda_2\ \vartheta\right] = \left[0.65\ 0.5\ 0.3\right]$ of corresponding map. In the same way the values of $M_S(M_t)$, N and IAE can be found in Figs. 10, 11 and 12, respectively.

The assessment of the controller tuning has been performed in terms of the dimensionless form of the control loop model (48). Now it is necessary *to convert* these results back into the original dimensional plant (105). Quite simple the conversion is for the proportional controller gain, from (21) $\rho_P = Kr_P$ and then the controller setting is $r_P = \rho_P/K = 0.7769$. For the other gains the time scale is given by $\sqrt[3]{c_3} = 2\ [s]$. Due to (21) the following setting of the rest of controller gains and filter time constant results

$$\begin{aligned} r_D &= \frac{\rho_D}{K}\sqrt[3]{8} = 2.5335\ [s], \\ r_I &= \frac{\rho_I}{K\sqrt[3]{8}} = 0.2902\ \left[s^{-1}\right], \\ T_f &= \tau\sqrt[3]{8} = 0.334\ [s] \end{aligned} \quad (111)$$

In converting the controller parameters back to the specific values also the prescribed natural frequency of the control loop is obtained. Using the scaling factor $\sqrt[3]{c_3} = 2\ [s]$ the natural frequency Ω of the control loop is $\Omega \equiv \omega_K = \nu_K/\sqrt[3]{c_3} = 0.534\ \left[s^{-1}\right]$ where the ultimate frequency number is $\nu_K = 1.068$. The corresponding prescribed *dimensional* poles are as follows $p_{1,2} = -0.1468 \pm j0.534$, $p_{3,4} = -0.2129 \pm j0.1935$.

The dominance of the prescribed poles $\bar{p}_1, \bar{p}_2, \bar{p}_3, \bar{p}_4$ has been checked by means of increment argument rule (99) in Fig. 19, where the ratio β_m/β is chosen 1.2. From the argument increment $-3\pi/2$ it is confirmed that to the right from line $\mathcal{L}$, $\bar{s} = -\beta_m + j\omega$, with $\beta_m = 0.511$ does not lie any pole except the quadruple $\bar{p}_{1,2,3,4}$. Applying the quasi-polynomial root finder from [61] the rightmost pole spectrum is evaluated in Figs. 20 and 21. In Fig. 21 the first five rightmost poles are drawn together with plant pole spectrum to evaluate both the dominance index according to (103) as $p_5/\mathrm{Re}\,(p_4) = \sigma = 17$ and the near-to dominant pole-zero cancellation. This shows both the abundant four-pole dominance and no dominant pole-zero cancellation.

Remark 3: An example of plant type (1) with the same similarity numbers, as in case of plant (105), but with different scaling factor is given as follows

$$11.18\frac{d^3y(t)}{dt^3} + 10\frac{d^2y(t)}{dt^2} + 3.44\frac{dy(t)}{dt} + y(t) = 0.8\,u(t-0.67) \quad (112)$$

for which the same control loop parameters (110) are valid but due to different scaling factor, $\sqrt[3]{c_3} = \sqrt[3]{11.18} = \sqrt[3]{\sqrt{125}} = \sqrt[3]{\sqrt{5^3}} = \sqrt{5} = 2.236\ [s]$, the *dimensional* gains r_D and

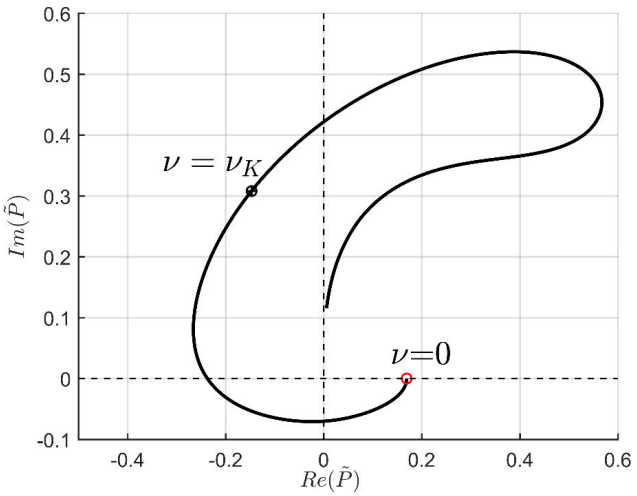

FIGURE 19. Function (102) hodograph with argument increment limit $-3\pi/2$ in case of plant (107).

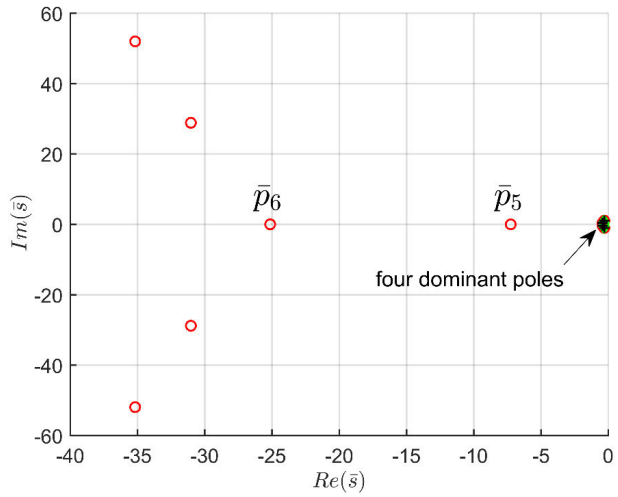

FIGURE 20. The separation of four rightmost poles from the rest of infinite spectrum in case of plant (107).

r_I result differently from (111), thus

$$r_D = \frac{\rho_D}{K}\sqrt[3]{5} = 2.5335\ [s]\,,\ r_I = \frac{\rho_I}{K\sqrt[3]{5}} = 0.2902\ \left[s^{-1}\right],$$
$$T_f = \tau\sqrt{5} = 0.3733\ [s] \tag{113}$$

In other words the common loop description by dimensionless model (107) together with universal real controller tuning (110) is unique not only for oscillatory plants (105) and (112) but also for the rest of plants with common similarity numbers (106). However, due to various scaling factors the control loop responses in time and frequency domain are different, e.g. disturbance rejection response in case of plant (105) differs from that response belonging to plant (112), additionally to different time delay (despite both plants have common laggardness number ϑ).

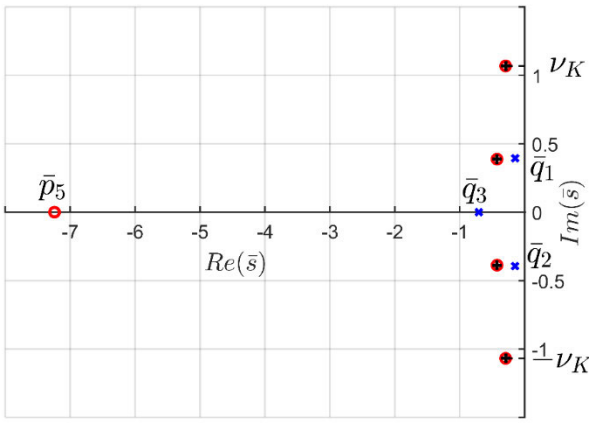

FIGURE 21. Rightmost spectrum belonging to proposed setting for plant (107), including plant pole option (5) in *blue x*.

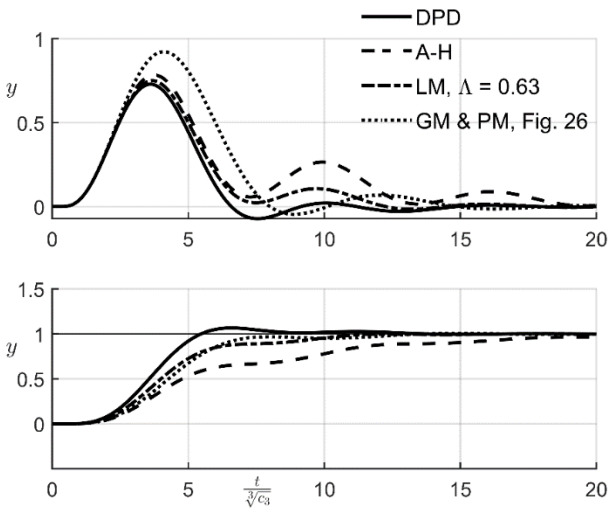

FIGURE 22. Comparative study for benchmark plant model (107); upper part – disturbance rejection responses, bottom part – reference tracking responses.

B. CONTROL LOOP PERFORMANCE AND ROBUSTNESS FOR BENCHMARK OSCILLATORY MODEL

In Table 1 the tuning methods considered are compared with respect to the performance criterion IAE, constraints on robustness and ratio N kept, and in Fig. 22 the disturbance rejection responses corresponding to the tuning methods compared are recorded for $N \leq 10$. The disturbance considered is the input disturbance loading the control loop according to the scheme in Fig. 4 by variable d which is the unit step function starting at origin in Fig. 22. Additionally, in bottom part of Fig. 22 using the control scheme in Fig. 4 the reference tracking responses are added to demonstrate that the dominant four-pole placement method provides quite good performance in comparison with other tuning methods although the proposed method optimizes the control loop preferably for the load disturbance rejection. In all the considered tuning methods for comparison the reference variable prefilter results with the damping factor at least 0.5 and the measurement filter time constant results

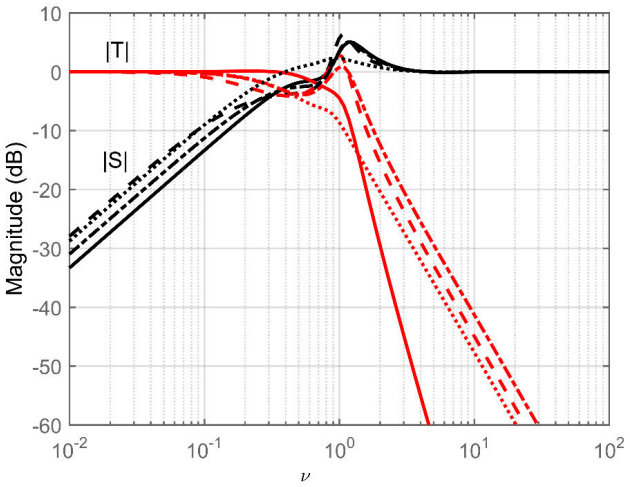

FIGURE 23. Magnitude frequency characteristics with legend from Comparative study in Fig. 22.

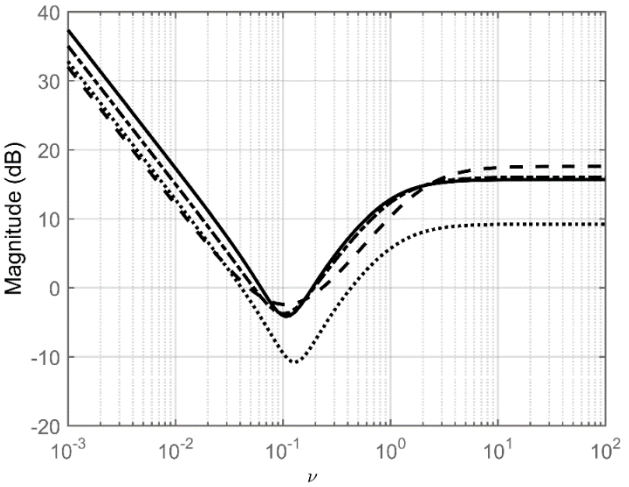

FIGURE 25. Controller (43) magnitude frequency characteristics with legend from Comparative study in Fig. 22.

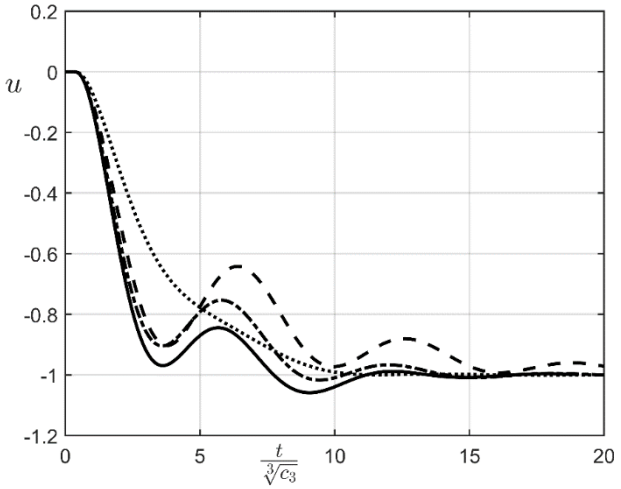

FIGURE 24. Control signal for load disturbance rejection from Comparative study in Fig. 22.

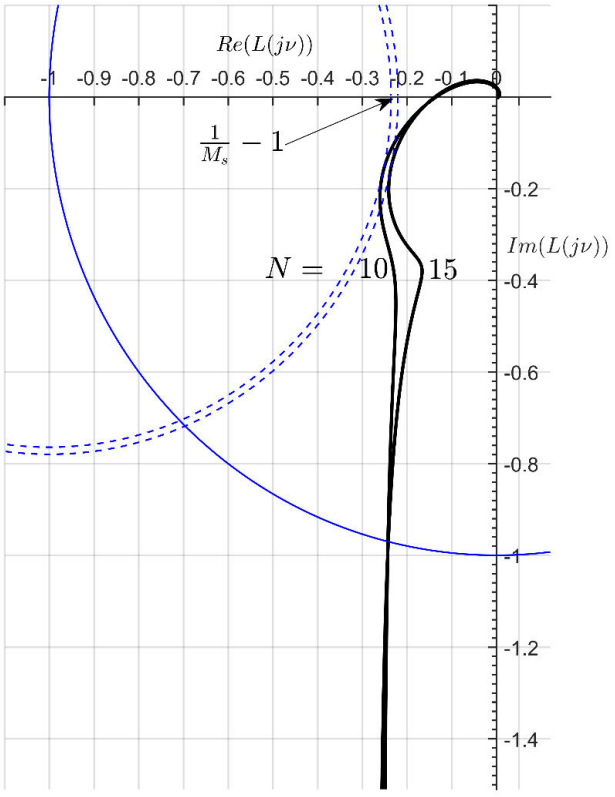

FIGURE 26. Nyquist plot showing gain and phase margin for GM & PM tunings from Table 1.

at least 10^{-1} [s]. The following abbreviations are used to indicate the compared controller tuning methods: DPD – dominant pole design (dominant four-pole placement method proposed in Section IV), LM – lambda tuning method, [35], A-H – Åström-Hägglund tuning method, and GM & PM – gain and phase margin optimization approach.

Based on the results recorded in Fig. 22 and the data in Table 1 the best PID tuning from the considered ones results the DPD which gives the lowest IAE value under the comparable robustness in the extreme frequency equivalence sense (Fig. 23). Also checking the control signal for the load disturbance rejection in Fig. 24 the DPD superiority is observed. With LM method, $\Lambda = 0.52$, the same IAE is achieved but with rather high maximum sensitivity $M_S = 2.023$. According to the GM & PM optimization, see Fig. 26, M_S results lower than in case of the proposed DPD, see Table 1, but the IAE results greater by 50%. The reason why the DPD results well in the IAE consists in the highest value of the integration gain obtained over all the considered tuning methods tailored to the third-order plants with delay. Moreover, the high-frequency control sensitivity results quite limited in comparison to other tuning methods, only GM & PM optimization leads to lower sensitivity than the DPD, see Fig. 25. Thus the high-frequency gain, M_u, results for tunings from Table 1 and $N \leq 10$ as follows: 6.215, 7.546, 6.477, 7.675, and 2.898 for DPD, A-H, LM ($\Lambda = 0.63$),

TABLE 1. Comparative study of real PID tuning rules and methods.

Control loop gains and filter time constant for benchmark plant model (107)								
Filter ratio	$N \leq 10$							
Parameter	ρ_P	ρ_D	ρ_I	τ	IAE	M_S	M_t	M_u
DPD[1] - proposed	**0.6215**	**1.0134**	**0.4643**	**0.1670**	**2.522**	**1.790**	**1.074**	**6.215**
A-H	0.7546	0.5703	0.2496	0.0753	4.006	2.077	1.387	7.546
LM, $\Lambda = 0.63^{\dagger}$	0.6477	0.8737	0.3546	0.1381	2.886	1.796	1.095	6.477
LM, $\Lambda = 0.52^{\dagger}$	0.7675	1.0353	0.4202	0.1381	2.524	2.023	1.356	7.675
GM & PM‡	0.2898	0.4188	0.2745	0.1445	3.839	1.309	1	2.898
Filter ratio	$N \leq 15$							
DPD[2] - proposed	**0.6724**	**1.0702**	**0.5401**	**0.1101**	**2.404**	**1.799**	**1.117**	**9.716**
A-H	0.7707	0.5776	0.2571	0.0509	3.889	2.071	1.395	11.350
LM, $\Lambda = 0.575^{\dagger}$	0.6851	0.9182	0.3846	0.0927	2.676	1.796	1.116	9.902
LM, $\Lambda = 0.492^{\dagger}$	0.7854	1.0526	0.4409	0.0927	2.401	1.969	1.314	11.351
GM & PM‡	0.2935	0.5156	0.2870	0.1171	3.585	1.283	1	4.403

[1] $\delta = 0.275$, $\kappa = 1.45$, and $\eta = 0.3625$
[2] $\delta = 0.29$, $\kappa = 1.4$, and $\eta = 0.425$
† Tuning from [35] is modified for application of filter (18).
‡ GM = 7.5, PM = 75º, see Fig. 26

LM ($\Lambda = 0.52$), and GM & PM, respectively. Values of M_u in both cases, $N \leq 10$ and $N \leq 15$, are also included into the Table 1. Naturally, the DPD cannot be in competition with LM as regards the reference tracking capability due to arbitrarily short lambda parameter (Λ) tuning if no actuator limitations are exceeded. Of course, the LM method then gives better IAE than the DPD but in the expense of robustness, see Table 1.

For other tuning methods, A-H and GM & PM optimization, similarly resulting reference tracking responses can be observed but with rather longer settling times. Notice that in Fig. 26 open loop transfer function $L(\bar{s})$ is evaluated for $\bar{s} = j\nu, \ \nu \in \langle 10^{-2}, 10^{3} \rangle$. In Table 1 one can also observe analogous results in favor of the DPD where all the tunings, robustness and performance measures are made for $N \leq 15$. With rising N under keeping the same M_S one can observe gradual decreasing the IAE, in general, while M_u is gradually increasing. Additionally increasing N over 20 already leads to implementation issues due to the demand on the sampling period of order less than 10^{-3} [s]. Particularly this is the case of A-H and LM tuning methods.

Remark 4: Naturally the notion of extreme frequency equivalence is not applicable to the A-H tuning method and also to the GM & PM optimization that has the capability to minimize the IAE at lower M_S than 1.8.

VII. DISCUSSION OF RESULTS

The universal PID and filter settings are proposed giving rise to optimum controller gains and measurement filter time constant with respect to not only the IAE criterion but also to the robustness and filtering effect constraints. The universality of the real controller settings consists in the control loop description via the similarity theory which imparts the control loop responses similar dynamics characterized by the similarity numbers. These responses differ from each other only in their scales of time and input and output variables. Consequently, for all the dynamically similar plants the same controller parameters ρ_P, ρ_D, ρ_I, τ are obtained from (54) through (57) and the four-pole dominance check according to the condition (99) holds for all of them in spite of the significant plant delay effect characterized by varying laggardness number ϑ. These controller and filter parameters are evaluated for optimum values of damping, root, and natural frequency ratios. Particularly the optimum natural frequency ratio, η, results nearly everywhere between 0.3 and 0.5 as shown in Fig. 16 to achieve the robust PID setting with sufficient performance. Additionally, to limit the high-frequency control sensitivity the measurement filter's ratio is constrained as $N \leq 15$. Despite the disturbance rejection optimization is preferred to that of the reference tracking the reference tracking capability is saved by prefiltering the reference variable in the classical control loop in Fig. 4. Simultaneously the dominant four-pole placement technique is extended for integrating third-order plants with delay.

The robustness constraint is achieved, as shown in Fig. 10, when the quadruple of dominant poles is assigned as two pairs of complex conjugate poles. Corresponding optimum controller gains and filter time constants are presented in Figs. 6-9. The dominance of the quadruple of assigned poles results abundant because the dominance index, recorded in Fig. 13, is nearly ten times greater than it is in usual dominant four-pole placement ($\sigma = 2$, see [30]). Thus, there are two natural frequencies assigned where one of them is the ultimate frequency to guarantee good disturbance rejection performance and the second one is new optimized via prescribing η to meet the robustness constraint as $M_S \leq 1.8$. The rest of ratios, δ and κ, are prescribed accordingly to keep not only the robustness constraint but also the high-frequency control sensitivity constrained by the filter's ratio as $5 < N < 20$. While ratios δ, κ are varying particularly with λ_2 the ratio, η, results in 0.35 as an average value across all the considered plants in case of both $\vartheta = 0.3$, see Fig. 16, and $\vartheta = 0.5$. Keeping $N \leq 10$, thus in the aforementioned range, under properly selected δ, κ and η in Fig. 14, 15 and 16, respectively, the filter time constant results in feasible, i.e. positive, number. Due to the enhanced delay effect, $\vartheta > 0.5$, and poor plant damping,

$\lambda_2 > 0.5$, the loop amplification is vanishing and the PID type control due to the scheme in Fig. 4 loses a potential to compensate for such stringent dynamics. Hence these cases with a poor chance of PID control application are excluded from the survey maps achieved. Finally, the separation of the dominant poles assigned from the rest of the infinite spectrum is considerable guaranteeing the desired control loop dynamics, and simultaneously the measurement filter's pole location falls into this rest preventing the dominant pole-zero cancellation.

The applicability range of the proposed method, DPD, is mainly in the field of the mechanical systems with actuator dynamics (e.g. servomechanism to pull a cart), thermal processes (e.g. heat exchanger), water turbines with long conduit etc. Other applications can be found in steel and energy industry.

VIII. CONCLUSION

The proposed dominant four-pole placement method gives rise to introduce novel tuning method for the real PID controller considered in application to the class of the third-order plants with delay parameterized according to the similarity theory. The delayed control loop results in the retarded system described by the fifth-order differential equation with delayed argument. Nevertheless, the real PID controller tuned due to the dominant four-pole placement is robust with sufficient performance for the practice and the four-pole dominance is guaranteed due to optimally prescribed ratios, particularly the natural frequency ratio. The comparative study, summarized in Table 1, for the benchmark oscillatory model shows the capability of the proposed dominant-four pole placement technique in contrast to other tuning and optimization methods.

REFERENCES

[1] Z. Shafiei and A. T. Shenton, "Tuning of PID-type controllers for stable and unstable systems with time delay," *Automatica*, vol. 30, no. 10, pp. 1609–1615, Oct. 1994, doi: 10.1016/0005-1098(94)90100-7.

[2] A. O'Dwyer, *Handbook of PI and PID Controller Tuning Rules*, 3rd ed. London, U.K.: Imperial College Press, 2009.

[3] S. Das, K. Halder, and A. Gupta, "Performance analysis of robust stable PID controllers using dominant pole placement for SOPTD process models," *Knowl.-Based Syst.*, vol. 146, pp. 12–43, Apr. 2018, doi: 10.1016/j.knosys.2018.01.030.

[4] R. C. Panda, C. C. Yu, and H. P. Huang, "PID tuning rules for SOPDT systems: Review and some new results," *ISA Trans.*, vol. 43, no. 2, pp. 283–295, Apr. 2004, doi: 10.1016/S0019-0578(07)60037-8.

[5] W. K. Ho, O. P. Gan, E. B. Tay, and E. L. Ang, "Performance and gain and phase margins of well-known PID tuning formulas," *IEEE Trans. Control Syst. Technol.*, vol. 4, no. 4, pp. 473–477, Jul. 1996, doi: 10.1109/87.508897.

[6] W. K. Ho, K. W. Lim, and W. Xu, "Optimal gain and phase margin tuning for PID controllers," *Automatica*, vol. 34, no. 8, pp. 1009–1014, 1998, doi: 10.1016/S0005-1098(98)00032-6.

[7] L. M. Eriksson and M. Johansson, "PID controller tuning rules for varying time-delay systems," in *Proc. Amer. Control Conf.*, New York, NY, USA, Jul. 2007, pp. 619–625.

[8] O. Garpinger, T. Hägglund, and K. J. Åström, "Performance and robustness trade-offs in PID control," *J. Process Control*, vol. 24, no. 5, pp. 568–577, May 2014, doi: 10.1016/j.jprocont.2014.02.020.

[9] P. Persson and K. J. Åström, "Dominant pole design–a unified view of PID controller tuning," in *Adaptive Systems in Control and Signal Processing*, Oxford, U.K.: Pergamon Press, vol. 1993, pp. 377–382.

[10] K. J. Åström, T. Hägglund, C. C. Hang, and W. K. Ho, "Automatic tuning and adaptation for PID controllers—A survey," *Control Eng. Pract.*, vol. 1, no. 4, pp. 699–714, Aug. 1993, doi: 10.1016/0967-0661(93)91394-C.

[11] H. B. J. Derbel, "Design of PID controllers for time-delay systems by the pole compensation technique," in *Proc. 6th Int. Multi-Conf. Syst., Signals Devices*, Djerba, Tunisia, Mar. 2009, pp. 1–6.

[12] M. Shamsuzzoha, S. Lee, and M. Lee, "Analytical design of PID controller cascaded with a lead-lag filter for time-delay processes," *Korean J. Chem. Eng.*, vol. 26, no. 3, pp. 622–630, May 2009, doi: 10.1007/s11814-009-0104-z.

[13] P. K. Medarametla and V. L. N. Komanapalli, "Maximum sensitivity based new PID controller tuning for integrating systems using polynomial method," *Chem. Product Process Model.*, vol. 12, no. 3, Apr. 2017, Art. no. 20160070, doi: 10.1515/cppm-2016-0070.

[14] Q.-G. Wang, M. Liu, and C. C. Hang, "Approximate pole placement with dominance for continuous delay systems by PID controllers," *Can. J. Chem. Eng.*, vol. 85, no. 4, pp. 549–557, May 2008, doi: 10.1002/cjce.5450850416.

[15] S. Das, K. Halder, and A. Gupta, "Delay handling method in dominant pole placement based PID controller design," *IEEE Trans. Ind. Informat.*, vol. 16, no. 2, pp. 980–991, Feb. 2020, doi: 10.1109/TII.2019.2918252.

[16] K. Halder, S. Das, and A. Gupta, "Time delay handling in dominant pole placement with PID controllers to obtain stability regions using random sampling," *Int. J. Control*, vol. 18, pp. 1–22, May 2020, doi: 10.1080/00207179.2020.1764110.

[17] P. Zítek and J. Fišer, "A universal map of three-dominant-pole assignment for PID controller tuning," *Int. J. Control*, vol. 93, no. 9, pp. 2267–2274, Sep. 2020, doi: 10.1080/00207179.2018.1554267.

[18] K. J. Åström and T. Hägglund, *PID Controllers: Theory, Design, and Tuning*, 2nd ed. Research Triangle Park, NC, USA: Instrument Society of America, 1995.

[19] S. Alcántara, R. Vilanova, and C. Pedret, "PID control in terms of robustness/performance and servo/regulator trade-offs: A unifying approach to balanced autotuning," *J. Process Control*, vol. 23, no. 4, pp. 527–542, Apr. 2013, doi: 10.1016/j.jprocont.2013.01.003.

[20] B. B. Alagoz, F. N. Deniz, C. Keles, and N. Tan, "Disturbance rejection performance analyses of closed loop control systems by reference to disturbance ratio," *ISA Trans.*, vol. 55, pp. 63–71, Mar. 2015, doi: 10.1016/j.isatra.2014.09.013.

[21] S. Alcántara, C. Pedret, and R. Vilanova, "On the model matching approach to PID design: Analytical perspective for robust servo/regulator tradeoff tuning," *J. Process Control*, vol. 20, no. 5, pp. 596–608, Jun. 2010, doi: 10.1016/j.jprocont.2010.02.011.

[22] T. B. Sekara and M. R. Matausek, "Optimization of PID controller based on maximization of the proportional gain under constraints on robustness and sensitivity to measurement noise," *IEEE Trans. Autom. Control*, vol. 54, no. 1, pp. 184–189, Jan. 2009, doi: 10.1109/TAC.2008.2008359.

[23] R. H. Middleton and S. F. Graebe, "Slow stable open-loop poles: To cancel or not to cancel," *Automatica*, vol. 35, no. 5, pp. 877–886, May 1999, doi: 10.1016/S0005-1098(98)00220-9.

[24] A. J. Isaksson and S. F. Graebe, "Analytical PID parameter expressions for higher order systems," *Automatica*, vol. 35, no. 6, pp. 1121–1130, Jun. 1999, doi: 10.1016/S0005-1098(99)00009-6.

[25] T. Liu and F. Gao, "New insight into internal model control filter design for load disturbance rejection," *IET Control Theory Appl.*, vol. 4, no. 3, pp. 448–460, Mar. 2010, doi: 10.1049/iet-cta.2008.0472.

[26] Y. Li, A. Sheng, and Q. Qi, "Further results on guaranteed dominant pole placement with PID controllers," in *Proc. 30th Chin. Control Conf.*, Yantai, China, Jul. 2011, pp. 3756–3760.

[27] V. R. Segovia, T. Hägglund, and K. J. Åström, "Measurement noise filtering for PID controllers," *J. Process Control*, vol. 24, no. 4, pp. 299–313, Apr. 2014, doi: 10.1016/j.jprocont.2014.01.017.

[28] A. D. Micić and M. R. Mataušek, "Optimization of PID controller with higher-order noise filter," *J. Process Control*, vol. 24, no. 5, pp. 694–700, May 2014, doi: 10.1016/j.jprocont.2013.10.009.

[29] V. R. Segovia, T. Hägglund, and K. J. Åström, "Measurement noise filtering for common PID tuning rules," *Control Eng. Pract.*, vol. 32, pp. 43–63, Nov. 2014, doi: 10.1016/j.conengprac.2014.07.005.

[30] J. Fišer, P. Zítek, and T. Vyhlídal, "Dominant four-pole placement in filtered PID control loop with delay," in *Proc. 20th IFAC World Congress*, Toulouse, France, 2017, pp. 6501–6506.

[31] A. Leva and M. Maggio, "A systematic way to extend ideal PID tuning rules to the real structure," *J. Process Control*, vol. 21, no. 1, pp. 130–136, Jan. 2011, doi: 10.1016/j.jprocont.2010.10.014.

[32] S. Skogestad, "Simple analytic rules for model reduction and PID controller tuning," *J. Process Control*, vol. 13, no. 4, pp. 291–309, Jun. 2003, doi: 10.1016/S0959-1524(02)00062-8.
[33] B. Kristiansson and B. Lennartson, "Evaluation and simple tuning of PID controllers with high-frequency robustness," *J. Process Control*, vol. 16, no. 2, pp. 91–102, Feb. 2006, doi: 10.1016/j.jprocont.2005.05.006.
[34] B. Kristiansson and B. Lennartson, "Robust tuning of PI and PID controllers: Using derivative action despite sensor noise," *IEEE Control Syst.*, vol. 26, no. 1, pp. 55–69, Feb. 2006, doi: 10.1109/MCS.2006.1580154.
[35] G. Marchetti and C. Scali, "Use of modified relay techniques for the design of model-based controllers for chemical processes," *Ind. Eng. Chem. Res.*, vol. 39, no. 9, pp. 3325–3334, Jul. 2000, doi: 10.1021/ie990657x.
[36] N. Hohenbichler, "All stabilizing PID controllers for time delay systems," *Automatica*, vol. 45, no. 11, pp. 2678–2684, Nov. 2009, doi: 10.1016/j.automatica.2009.07.026.
[37] D.-J. Wang, "Synthesis of PID controllers for high-order plants with time-delay," *J. Process Control*, vol. 19, no. 10, pp. 1763–1768, Dec. 2009, doi: 10.1016/j.jprocont.2009.07.012.
[38] V. A. Oliveira, L. V. Cossi, M. C. M. Teixeira, and A. M. F. Silva, "Synthesis of PID controllers for a class of time delay systems," *Automatica*, vol. 45, no. 7, pp. 1778–1782, Jul. 2009, doi: 10.1016/j.automatica.2009.03.018.
[39] K. Saadaoui, S. Elmadssia, and M. Benrejeb, "Stabilizing PID controllers for a class of time delay systems," in *PID Controller Design Approaches-Theory, Tuning and Application to Frontier Areas*, M. Vagia, Ed. Rijeka, Croatia: IntechOpen, 2012, ch. 7, pp. 141–158.
[40] T.-H. Pan, Y. Le, and S.-Y. Li, "Multiple model-based predictive control for the plant-wide thermal processes," *Syst. Eng. Electron.*, vol. 26, no. 10, pp. 1439–1443, 2004.
[41] P. Hušek, "PID controller design for hydraulic turbine based on sensitivity margin specifications," *Int. J. Electr. Power Energy Syst.*, vol. 55, pp. 460–466, Feb. 2014, doi: 10.1016/j.ijepes.2013.09.029.
[42] M. A. Poller, "Doubly-fed induction machine models for stability assessment of wind farms," in *Proc. IEEE Bologna Power Tech Conf.*, Bologna, Italy, Jun. 2003, pp. 1–6.
[43] C. Yanqiao, L. Liheng, and C. Hainan, "Research and designing of boiler-turbine model linearization balance operating point based on energy-saving and non-linear measurement analysis," in *Proc. 38th Annu. Conf. IEEE Ind. Electron. Soc. (IECON)*, Montreal, QC, Canada, Oct. 2012, pp. 1145–1149.
[44] W. Tan, "Tuning of PID load frequency controller for power systems," *Energy Convers. Manage.*, vol. 50, no. 6, pp. 1465–1472, Jun. 2009, doi: 10.1016/j.enconman.2009.02.024.
[45] C. D. Johnson, "A family of linear, time-invariant universal adaptive controllers for linear and non-linear plants," *Int. J. Control*, vol. 49, no. 4, pp. 1217–1233, Apr. 1989, doi: 10.1080/00207178908559702.
[46] K. J. Åström and T. Hägglund, "Benchmark systems for PID control," in *Proc. Digit. Control-Past, Present Future PID Control (IFAC)*, Terrassa, Spain, 2000, pp. 165–166.
[47] A. Bartoszewicz and A. Nowacka, "Sliding-mode control of the third-order system subject to velocity, acceleration and input signal constraints," *Int. J. Adapt. Control Sig. Proc.*, vol. 21, nos. 8–9, pp. 779–794, Oct./Nov. 2007, doi: 10.1002/acs.970.
[48] K. J. Åström, H. Panagopoulos, and T. Hägglund, "Design of PI controllers based on non-convex optimization," *Automatica*, vol. 34, no. 5, pp. 585–601, May 1998, doi: 10.1016/S0005-1098(98)00011-9.
[49] H. Panagopoulos, K. J. Åström, and T. Hägglund, "Design of PID controllers based on constrained optimisation," *IEE Proc.-Control Theory Appl.*, vol. 149, no. 1, pp. 32–40, Jan. 2002, doi: 10.1049/ip-cta:20020102.
[50] J.-C. Shen, "New tuning method for PID controller," *ISA Trans.*, vol. 41, no. 4, pp. 473–484, Oct. 2002, doi: 10.1016/S0019-0578(07)60103-7.
[51] N. N. Ivashchenko, *Automatic Control: System Theory and elements*. Moscow, Russia: MASHGIZ, 1962.
[52] V. L. Kharitonov, S.-I. Niculescu, J. Moreno, and W. Michiels, "Static output feedback stabilization: Necessary conditions for multiple delay controllers," *IEEE Trans. Autom. Control*, vol. 50, no. 1, pp. 82–86, Jan. 2005, doi: 10.1109/TAC.2004.841137.
[53] O. Garpinger, "Design of robust PID controllers with constrained control signal activity," Ph.D. dissertation, Dept. Autom. Control, Lund Univ., Lund, Sweden, 2009.
[54] O. Garpinger and T. Hägglund, "Software-based optimal PID design with robustness and noise sensitivity constraints," *J. Process Control*, vol. 33, pp. 90–101, Sep. 2015, doi: 10.1016/j.jprocont.2015.06.001.
[55] P. Zítek, J. Fišer, and T. Vyhlídal, "Dimensional analysis approach to dominant three-pole placement in delayed PID control loops," *J. Process Control*, vol. 23, no. 8, pp. 1063–1074, Sep. 2013, doi: 10.1016/j.jprocont.2013.06.001.
[56] P. Zítek, J. Fišer, and T. Vyhlídal, "Dynamic similarity approach to control system design: Delayed PID control loop," *Int. J. Control*, vol. 92, no. 2, pp. 329–338, Feb. 2019, doi: 10.1080/00207179.2017.1354398.
[57] A. Ramírez, R. Sipahi, S. Mondié, and R. Garrido, "An analytical approach to tuning of delay-based controllers for LTI-SISO systems," *SIAM J. Control Optim.*, vol. 55, no. 1, pp. 397–412, 2017, doi: 10.1137/15M1050999.
[58] J. Fišer and P. Zítek, "PID controller tuning via dominant pole placement in comparison with Ziegler-Nichols tuning," in *Proc. 15th IFAC Workshop Time Delay Syst. (TDS)*, Sinaia, Romania, 2019, pp. 43–48.
[59] J. Fiser, P. Zitek, and V. Kucera, "IAE optimization of delayed PID control loops using dimensional analysis approach," in *Proc. 6th Int. Symp. Commun., Control Signal Process. (ISCCSP)*, Athens, Greece, May 2014, pp. 262–265.
[60] S. Das, S. Saha, S. Das, and A. Gupta, "On the selection of tuning methodology of FOPID controllers for the control of higher order processes," *ISA Trans.*, vol. 50, no. 3, pp. 376–388, 2011, doi: 10.1016/j.isatra.2011.02.003.
[61] T. Vyhlídal and P. Zítek, "Mapping based algorithm for large-scale computation of quasi-polynomial zeros," *IEEE Trans. Autom. Control*, vol. 54, no. 1, pp. 171–177, Jan. 2009, doi: 10.1109/TAC.2008.2008345.

JAROMÍR FIŠER received the M.S. degree in control and information engineering and the Ph.D. degree in technical cybernetics from Czech Technical University (CTU) in Prague, Czech Republic, in 1998 and 2004, respectively.

In 2000, he was a Junior Researcher with the Center of Applied Cybernetics, Research Group, CTU in Prague. Since 2017, he has been a Researcher with the Center of Aviation and Space Research, Faculty of Mechanical Engineering, CTU in Prague. Since 2021, he has been an Associate Professor in machine and process control with the Faculty of Mechanical Engineering, CTU in Prague. His main research interests include analysis and synthesis of time delay systems and industrial process control. His applied research areas are control solutions in steel and energy generation industry and cultural heritage preservation. He is an Associate Editor of *Kybernetika* journal and holds three licensed software.

PAVEL ZÍTEK was born in Prague, Czech Republic, in 1939. He received the M.S. degree in precise mechanics and optics, the Ph.D. degree in technical cybernetics, and the D.Sc. degree in technical cybernetics from Czech Technical University (CTU) in Prague, Czech Republic, in 1961, 1968, and 1987, respectively. His Ph.D. dissertation was entitled Anisochronic Dynamic Systems.

Since 1990, he has been a Professor in technical cybernetics at the Faculty of Mechanical Engineering, CTU in Prague. Since 1990, he has been the Director of the Department of Automatic Control and Engineering Informatics, CTU in Prague. Since 2000, the Head of the Research Group at the Centre of Applied Cybernetics, CTU in Prague. He is the author of three books, eight book chapters, and more than 250 articles. His H-index is 13 and his most cited works range mostly over the area of analysis and synthesis of time delay systems, namely An Observer Design for Linear Time-Delay Systems, IEEE TRANSACTIONS ON AUTOMATIC CONTROL, in 2002, Algebraic Design of Anisochronic Controllers for Time Delay Systems, *International Journal of Control*, in 2003, and Dimensional Analysis Approach to Dominant Three-Pole Placement in Delayed PID Control Loops, *Journal of Process Control*, in 2013. His research interests also include topics on airliner cabin air-conditioning and systems of air-conditioning for cultural heritage preservation. He is a member of the Editorial Board of *Kybernetika* journal. His works in these topics have been published in *Building and Environment* journal. He was a recipient of the Rector's Award for Excellent Research at the Faculty of Mechanical Engineering, CTU in Prague, in 2010.